Astron. Astrophys. 183, 295–313 (1987)

ASTRONOMY
AND
ASTROPHYSICS

Radiation driven winds of hot luminous stars

III. Detailed statistical equilibrium calculations for hydrogen to zinc

A. Pauldrach

Universitäts-Sternwarte München, Scheinerstr. 1, D-8000 München 80, Federal Republic of Germany

Received August 8, 1986; accepted February 16, 1987

Summary. Detailed multi-level statistical equilibrium calculations for the dominant ions of H to Zn in hot star stellar winds are presented. The calculations comprise in total *133 ionization stages of 26 elements with altogether 4000 levels and 10,000 radiative bound-bound transitions based on the line list of Abbott (1982)*. Electron collisions are included and the correct continuous radiation field obtained from the solution of the spherical transfer equation is taken into account for the bound-free transitions, thus avoiding the approximation of overall optically thin geometrically diluted continua. The statistical equilibrium is treated self-consistently together with the improved hydrodynamics of radiation driven cool winds (see Pauldrach et al., 1986), where the statistical equilibrium occupation numbers include the contribution of more than 100,000 lines to the line force. The calculations are applied on two objects, the O4f-star ζ Pup and the O9.5V-star τ Sco. The results are:

1. Non-LTE multi-level effects are extremely important. Previous gaseous nebula-like approximations do not lead to a quantitatively correct description. The most important difference is a significant shift to higher ionization stages. This is mainly caused by the optical thick ionization continuum shortward of the He II edge and in the lower part of the wind by collisional excitation of low lying excited levels and subsequent photoionization from these levels.

2. High ionization species like O VI, S VI, N V etc. can be easily produced in a cool wind model for ζ Pup. *Thus the longstanding problem of "superionization" can be solved without any other source of ionization.* For τ Sco the calculations produce sufficient N V, but fail marginally for O VI.

3. For excited levels – in particular for very strong resonance lines – the collision free two-level approximation turns out to be poor for particles densities higher than $10^{10}\,\mathrm{cm}^{-3}$. This can have consequences for spectral diagnostics of stellar winds.

4. The back reaction of the improved occupation numbers on the wind dynamics is significant. The shift to higher ionization stages weakens the line force and leads for both objects to better agreement with the observations in the mass-loss rate and terminal velocity.

Key words: early-type stars – non-LTE – mass loss – winds

1. Introduction

The detailed knowledge about the physical conditions of ionization and excitation in the winds of hot stars is of basic importance, not only for their spectral diagnostics (determination of mass-loss rates, density and temperature stratification, abundances) but also for the self-consistent theoretical description of the stellar wind hydrodynamics. For the latter the most promising concept is the theory of radiation driven winds where the wind is initiated and maintained by absorption of photospheric photon momentum in thousands of UV spectral lines (Lucy and Solomon, 1970; Castor et al. ("CAK"), 1975; Abbott, 1979; Abbott, 1982). It is obvious that in the framework of this theory the correct computation of occupation numbers is crucial, since the driving force of the wind depends on correctly computed line absorption coefficients.

However, despite reasonable progress in the selfconsistent theory of radiation driven winds (Abbott, 1982; Friend and Castor, 1983; Abbott and Lucy, 1985; Pauldrach et al., 1986, (Paper I); Kudritzki et al., 1986, (Paper II)) it should be realised that in the past, the treatment of the occupation numbers has suffered from approximations which were used "ad hoc" without any further justification. For instance, in the calculation of the ionization equilibrium recombination theory with geometrically diluted photospheric radiation has been applied (for the two basic approaches see Abbott, 1982 and Abbott and Lucy, 1985). In view of the particle densities in stellar winds ($10^{12}\,\mathrm{cm}^{-3} \geq n_E \geq 10^{8}\,\mathrm{cm}^{-3}$) this is *a priori* questionable. Very similar approximations were also used in the spectral diagnostics of stellar winds (see for example Lamers and Morton, 1976; Lamers and Rogerson, 1978; Hamann, 1980, 1981).

The only way to check such ad hoc approximations is to treat the complete statistical equilibrium self-consistently for all important element species in the wind. Although this is a complex problem requiring an enormous organisational and computational effort, we have estimated that the solution is feasible with present day computer capacity. Consequently, in view of the principal importance of such calculations we have developed a code which, for a given photospheric and stellar wind structure, solves the detailed multi-level statistical equilibrium equations for the dominant ions of H to Zn self-consistently. *In total 133 ionization stages of 26 elements with altogether 4,000 levels are treated.* For every level the corresponding radiative bound-free transitions with the correct continuous radiation field obtained from the solution of the spherical transfer equation is taken into account thus avoiding the critical approximation of optically thin geometrically diluted continua. Besides electron collisions more than 10,000 radiative bound-bound transitions are included explicitly to give sufficiently realistic atomic models for the occupation numbers in question.

The initial velocity and density structure of the stellar wind are obtained from the radiation-driven wind code developed recently by our group. This code, because of major improvements in the calculation of the radiative line force, gives mass-loss rates $\dot{M}$ and terminal velocities v_∞, which are rather close to the observations not only for galactic OB stars (Paper I) but also for O stars in the Magellanic Clouds (Paper II) despite the approximative calculation of the occupation numbers. With the statistical equilibrium code described above new occupation numbers are obtained which allow the calculation of a new line force arising from the contribution of more than 100,000 lines in total. With this new line force the stellar wind code gives a new velocity and density structure and the process is iterated until convergence is achieved. The final model gives a completely self-consistent solution of the radiation hydrodynamic stellar wind problem in spherical geometry. The hydrodynamic equations which include the radiative line force and the statistical equilibrium equations for all relevant ions that contain the radiative transitions are fulfilled simultaneously.

This paper reports first results of such calculations which have been applied to two well observed standard stars, namely the O4f-star ζ Pup and the O9.5V-star τ Sco. With regard to the stages of ionization observed in their wind spectra both objects (as almost all O-stars) pose the interesting problem of "super-ionization". This simply indicates the presence of anomalously high stages of ionization like O VI and N V. Contrary to other authors who tried to explain the presence of such ions by the Auger-effect and an X-ray radiation field (arising from either a hot corona or randomly distributed shocks travelling through the wind) or by a "warm" wind model of 200 kK electron temperature, we will show that, at least for ζ Pup, "superionization" can also be obtained in the simplest case of a "cool" wind model (where the electron temperature T_e is of the order of the effective temperature $T_{\rm eff}$) if only the statistical equilibrium is correctly handled. As the recent IR-observations of stellar winds strongly point to this cool wind model (Lamers et al., 1984), this is a very encouraging result. It demonstrates that the situation for the interpretation of the ionization conditions in hot star stellar winds is probably not as hopeless as commonly thought. The consequences of this will be discussed in Sect. 5. In Sect. 2 the choice of the cool wind model is justified in more detail and the alternative concepts that have been previously developed are also discussed. The details of the new statistical equilibrium calculations are described in Sect. 3 and in Sect. 4 the results with respect to ionization, excitation, line force and dynamics are presented and compared with previously used approximations.

2. Superionization and the choice of a wind model

As already mentioned in Sect. 1, one of the striking pecularities in the winds of hot luminous stars is the so-called "superionization". This term simply indicates the presence of anomalously high stages of ionization such as O VI and N V. The P Cygni profiles from resonance lines of these ionization stages have been observed with the Copernicus satellite for many O stars and B supergiants (see for instance Olson and Castor, 1981), so that attempts to explain this phenomenon are indispensable.

As can be easily verified, O VI cannot be explained by photoionization from the ground level of O V by the emergent flux from a static model atmosphere (Castor, 1979). The corresponding ionization rate is orders of magnitude too small to produce the high ionization species O VI and N V. Hence Lamers and Morton (1976) have introduced a "warm" wind model and suggest that the electron temperature in the wind lies in the range of 2000 kK so that O VI is mainly produced by collisional ionization. However, observations of infrared fluxes show that the electron temperature in the wind is closer to the effective temperature than to the high value of 200 kK (Lamers et al., 1984).

An alternative for the production of O VI and N V in O stars and B supergiants was proposed by Olson (1978), Cassinelli and Olson (1979) and Olson and Castor (1981). They use the X-ray emission from a thin hot corona ($T > 10^6$ K) at the base of a cool wind, the existence of which was first suggested by Hearn (1975), to produce O VI from O IV by photoionization due to the Auger process. Through the application of this model the above authors were able to reproduce the main features of the observed high ionization species of the elements He, C, N, O, Ne, Mg, Si and S. However, X-ray spectral observations by Long and White (1980) and Cassinelli and Swank (1983) show, at least for an O star (ζ Pup) and a B supergiant (ε Ori), that there is definitely far more flux below 1 keV than is predicted by the thin corona model. As shown by Cassinelli and Swank (1983) and discussed by Olson and Castor (1981) this model results in an inevitable attenuation of the X-ray flux in the wind and is thus in strong contradiction to observations.

Waldron (1984) has recently made an attempt to modify the theory of a thin corona at the base of the wind with a recombination stellar wind model. In order to decrease the stellar wind opacity at the K-shell edges Waldron has increased the coronal emission measure so that the ionic number densities and thus the opacities are reduced, whereas the mass column density is fixed. Consequently, Waldron's modified coronal model results are closer to the HEAO2-IPC observations, but compared with solid state spectrometer observations by Cassinelli and Swank (1983) Waldron's calculated oxygen K-shell absorption edge is still much too strong. Additionally, his calculated O VI ratio for ζ Pup is about 1 to 2 dex larger than observations indicate (Hamann, 1980; Lamers and Morton, 1976), whereas those of the low stages of ionization like N III, C III, which are also observed, are completely diminished. Thus it again seems questionable as to whether the coronal model is able to reproduce the main observational features of stellar winds, especially as Waldron states that the stellar wind and coronal zone must be in a delicate balance in order to reproduce the observed X-rays.

On the other hand, the semi-empirical theory of Lucy (1982) based on shocks distributed randomly in a "cool" wind and reaching far out into the terminal velocity region of the flow produces a stellar wind soft X-ray spectrum much closer to the observations. It is usually argued that the spectral superionization features such as O VI and N V might also be produced by the diffuse X-ray radiation field arising from the shocks in the wind.

However, without detailed knowledge about the physical properties of the shocks as function of distance from the stellar photosphere this is difficult to prove quantitatively. Only some qualitative considerations appear to be possible. According to Lucy the X-ray emission continues out into the terminal flow. The postshock temperature (T_s) increases proportionally to the velocity and the fit parameter v, which is defined as the difference in peak velocity between two successive shocks, divided by

the intershock sound speed ($v = \Delta v/a$). The lack of absorption at the K-shell edges in the observations can be interpreted, in view of Lucy's conclusions, as indicating that the bulk of the observed X-rays are emitted far out in the wind. This is also supported by Krolik and Raymond (1985) who showed that optically thin shocks, which are responsible for the X-ray emission, exist primarily in the upper part of the wind, whereas in the lower part of the wind optically thick shocks are more probable. The latter shocks emit mostly in the ultraviolet. With respect to Lucy's calculations this means that his parameter v also increases with velocity and thus T_s might be further reduced in the inner part of the wind. With this in mind, we have estimated the photoionization rate of the Auger effect for O VI with the assumption that the observed X-rays for ζ Pup arise from the regions where $v(r) \approx 0.9 v_\infty$ (the X-ray data were taken from Lucy and the cross section for K-shell ionization from Deltabuit and Cox, 1972). This rate was compared with the photoionization rate in the same region using the results of our detailed statistical equilibrium calculations (see Sects. 3 and 4), which at the moment assume a cool wind and ignore a probable diffuse X-ray radiation field. It was found that the rates are comparable. However, the mean intensity of our photoionization rate increases by several dex in the intermediate and inner part of the wind, whereas we expect the corresponding one for the diffuse X-ray Auger rate to remain constant or even to decrease for the reasons given above. This means, however, that the high ionization species *in the inner part of the wind* ($v < 0.9 v_\infty$) are possibly not created by Auger ionization. However, Auger ionization might influence the statistical equilibrium in the outermost part of the wind ($v > 0.9 v_\infty$). On the other hand additional ultraviolet radiation coming from optically thick shocks might contribute to the ionization balance.

In view of this somewhat uncertain situation we have restricted our calculations to the most simple case of pure "cool" wind models, i.e. models with a kinetic electron temperature T_e in the wind which is close to the photospheric effective temperature $T_{\rm eff}$. Since in the improved theory of radiation driven winds (Abbott and Lucy, 1985; Paper I; Paper II; Friend and Abbott, 1986) these models lead to mass-loss rates and terminal velocities very close to the observations and since IR-observations also seem to support this assumption (Lamers et al., 1984), we find it very attractive to investigate to what extent improved statistical equilibrium calculations for cool winds are already able to reproduce the observed distribution of ionization in stellar winds. As will become obvious from the following section, the code we have developed allows the incorporation of the Auger rates easily, once it is possible to specify the diffuse X-ray radiation field in more detail. The results of our calculations (Sect. 4) will show however that at least for the O4f-star ζ Pup this is not necessary.

3. The improved statistical equilibrium calculations

All previous calculations of ionization equilibrium in hot star stellar winds (except CAK, who used LTE) are based on "quasi-gaseous nebula approximations" assuming an optically thin geometrically diluted radiation field and neglecting bound-bound electron collisions. In addition, Abbott (1982) in his Eq. (8) has assumed that *all lines* are *optically thick* so that the occupation numbers are determined by direct recombination and ionization for each level (the same assumptions have been made for the wind models in Paper I and II). On the contrary, Abbott and Lucy (1985) assumed *all lines* to be *optically thin* for the calculation of ground state occupation numbers so that the ionization equilibrium in the wind resembles that in planetary nebulae. From the calculation of spectral lines for the line force based on such occupation numbers it is clear that roughly 50% to 70% of the line force is given by strong lines (optically thick), whereas the remaining force is given by weak lines (optically thin). Thus it is clear that both optically thick and thin lines exist in the wind and contribute to the dynamics. It is therefore reasonable that the ionization of elements will be affected by the presence of both optically thin and thick lines as well and a more detailed treatment is needed.

The complete neglect of bound-bound electron collisions in previous work also appears to be dangerous since the electron density in the accelerating region of the wind is between $10^{14}\,{\rm cm}^{-3}$ and $10^{10}\,{\rm cm}^{-3}$. In fact, the results of our calculations (Sect. 4) prove the importance of electron collisions which indirectly influence the ionization equilibrium significantly.

Another crucial test of the previous calculations concerns the assumption of optically thin geometrically diluted continua. Taking the occupation numbers from calculations either following Abbott (1982) or Abbott and Lucy (1985) it is easy to show for O-stars that the continuous radiation field becomes optically thick beyond the He II ground state absorption edge. Consequently, for ground state continua shortward of this edge ionization theory with continuum radiative transfer is needed (see also Castor, 1979). As we shall show below, this will have a dominating influence.

In the following part of this section we describe the details of our calculations which avoid all of the deficiencies mentioned above.

3.1. *The general iteration cycle*

Occupation numbers based on detailed statistical equilibrium calculations and corresponding line forces are calculated self-consistently with the radiation driven wind hydrodynamics. The iteration cycle is as follows:

i) Calculation of the density and velocity structure using our improved theory of radiation driven winds (see Paper I). For the first iteration the starting value for the line force is computed in the same way as described by Abbott (1982) and in Paper II.

ii) Based on i) the non-LTE multi-level rate equations are solved for all 26 elements in their different ionization stages. For this solution the continuum radiative transfer is correctly treated. Electron collisions are included. For the bound-bound radiative transitions the Sobolev approximation is used. (Details are given below).

iii) Based on ii) a new line force is calculated again using the Sobolev approximation (see Paper I). This line force is then parametrized in the same way as was done by Abbott (1982, see also Paper I and II) but allowing for stepwise radial changes of the fit parameters k, α, δ, which gives a more accurate representation of the line force. (Details are to be found in Pauldrach, 1986). With the new line force the iteration cycle starts again at i).

This scheme is used until convergence for $\dot{M}$ and v_∞ is achieved. The model is considered as to be converged when the relative deviations are less than 0.5%. The quantities used as

input are the atomic models including atomic data, the chemical composition, the photospheric flux, the temperature structure and the stellar parameters $T_{\rm eff}$, $\log g$, R_*.

3.2. Selection of elements, atomic models, chemical composition

The basis of our calculations is the line list published by Abbott (1982), which contains more than 250,000 lines of the first to sixth stages of ionization from H to Zn (see also Paper II).

In order to include only data in the calculations which are really needed, the level and the line list was reduced. The constraints for this reduction were:

(1) Only elements which yield more than 0.05% of the total line force have been considered. This results in 26 elements which were taken into account (see Appendix A and also Abbott (1982)).

(2) A maximum principal quantum number in each ionization stage was introduced up to which levels have been taken into account. This number was chosen so that

a) the total line force variations due to the reduction were less than 0.05% throughout the envelope;

b) the maximum number of levels for each ionization stage never exceeds 49. As the rate equations are solved simultaneously for three ionization stages and for the ground level of a fourth stage, this constraint is important for the accuracy of the matrix inversion (a matrix of a size greater than 150 × 150 is difficult to invert with high precision). When this constraint was in contradiction to a) the levels and lines were packed in a physically reasonable manner.

The calculations for this reduction were carried out using Abott's (1982) approximate formula (Eq. 8) for the occupation numbers. (The electron temperature T_e was varied between 10 kK to 50 kK).

The remaining ionization stages after the reduction are 133 in total. These take into account 3,824 levels, 9,043 combining lines and 104,878 lines for which the lower level is considered and thus contributes to the line force.

Details about the atomic structure of the elements and ionization stages considered in the calculations are given in Appendix A.

Solar abundances (Holweger, 1979) have been adopted for ζ Pup. For future work individual stellar abundances will be used based on detailed analyses of photospheric spectra; in the case of τ Sco the solar abundances have been scaled down (see Sect. 4.2) following the results of photospheric abundance analyses.

3.3. Rate equations

As customary for non-LTE investigations the basic assumption for the following considerations is that the populations are in statistical equilibrium. Despite the high outflow velocities this supposition is a reasonable one since the recombination time is small (Lamers and Morton, 1976; Lucy and Solomon, 1970; Klein and Castor, 1978).

The statistical equilibrium equations for collisional and radiative processes for each level i are:

$$-\sum_{j<i} n_j C_{ji} + n_i\left(\sum_{j<i}(n_j/n_i)^* C_{ji} + \sum_{j>i} C_{ij} + C_{ik}\right) - \sum_{j>i} n_j(n_i/n_j)^* C_{ij} - n_k(n_i/n_k)^* C_{ik} - \sum_{j<i} n_j R_{ji} + n_i\left(\sum_{j<i} R_{ij} + \sum_{j>i} R_{ij} + R_{ik}\right) - \sum_{j>i} n_j R_{ji} - n_k R_{ki} = 0 \qquad (1)$$

The letter k stands for continuum state and the notation $(\ )^*$ denotes the value that the quantity in parentheses has in thermodynamic equilibrium at the local electron temperature. Completing the system an additional equation is needed for each element K:

$$\sum_{r,l} n_{r,l} = Y_K N_H \qquad (2)$$

where l, r are the designations of level and ionization stage, respectively. Y_K is the element abundance relative to the hydrogen density N_H.

The collision rates C_{ij} (j may be bound or free) are calculated by

$$C_{ij} = n_E q_{ij}. \qquad (3)$$

The values chosen for q_{ij} are given in Appendix B. The radiative rates for bound-bound transitions are given by

$$R_{ij} = B_{ij}\bar{J}_{ij}$$
$$R_{ji} = A_{ji} + B_{ji}\bar{J}_{ij}, \qquad (4)$$

where A_{ji}, B_{ji} are the usual Einstein coefficients. $\bar{J}_{ij}$ is the angle-averaged, profile-weighted intensity of the radiation in the line transition.

As the envelope is in a state of rapid radial expansion, it is possible to use the escape-probability method in treating the transfer of line radiation developed by Castor (1970, see also Paper I). Then $\bar{J}_{ij}$ is given by

$$\bar{J}_{ij} = (1-\beta)S_{ij} + \beta_c I_c, \qquad (5)$$

where the line source function is

$$S_{ji} = \frac{n_j A_{ji}}{n_i B_{ij} - n_j B_{ji}}. \qquad (6)$$

In the case of optically thin continua at the frequency of the line transitions I_c is given by the emergent photospheric flux H_c

$$I_c = 4H_c(R). \qquad (7)$$

(In Eq. 7 photospheric limb darkening is neglected).

In the optically thick parts of the envelope the Sobolev approximation with continuum developed by Hummer and Rybicki (1985) should be used. However, as nearly all lines lie longward of the He II edge where for our two example stars the continuum is optically thin (see Sect. 4) this case is not important at the moment but could become crucial for W-R stars.

The escape probability functions β and β_c in Eq. (5) are given by the integrals

$$\beta = \int_0^1 \frac{1+\sigma x^2}{\tau_0}\left(1 - \exp\left(-\tau_0/(1+\sigma x^2)\right)\right) dx \qquad (8)$$

$$\beta_c = 1/2 \int_{\mu_c}^1 \frac{1+\sigma x^2}{\tau_0}\left[1 - \exp\left(-\tau_0/(1+\sigma x^2)\right)\right] dx$$

where

$$\sigma = rv'(r)/v(r) - 1$$
$$\mu_c = (1 - R^2/r^2)^{1/2} \qquad (9)$$

and the optical depth is defined by

$$\tau_0(r) = \frac{\pi e^2}{m_e c}(gf)_{ij}(n_i/g_i - n_j/g_j) rc/(v_0 v(r)). \qquad (10)$$

The statistical weights g, the oscillator strength f and the wavelength of the transitions ν_0 enter the last equation.

An additional remark is necessary regarding Eq. (5). The mean intensity in this form neglects changes through multi-line scattering. It is clear that this effect can influence the population of excited levels so that further modifications will be needed. Work in this direction is presently under way in our group.

The radiative rates for the bound free transitions are given by

$$R_{ik} = 4\pi \int_{\nu_i}^{\infty} \frac{\alpha_{ik}(\nu)}{h\nu} J_\nu \, d\nu$$

$$R_{ki} = \left(\frac{n_i}{n_k}\right)^* 4\pi \int_{\nu_i}^{\infty} \frac{\alpha_{ik}(\nu)}{h\nu} \left(\frac{2h\nu^3}{c^2} + J_\nu\right) \exp(-h\nu/kT_e)\, d\nu \,. \qquad (11)$$

(The choice of the photoionization cross-section $\alpha_{ik}(\nu)$ is described in Appendix B).

From the previous discussion we have to conclude that the winds of O-stars can be optically thick in the He II continuum. Therefore, in this case the stellar flux is attenuated by the optical depth and the continuum radiation field depends on the local electron temperature. The latter fact has a crucial influence on the ionization balance as will be seen in Sect. 4. As the transfer of radiation in the continua is hardly affected by the presence of a velocity field, the continuum is calculated from the static spherically symmetric transfer equation. Since it is neither possible nor necessary to include all ionization edges of the considered levels in the continua calculations, a choice of the important edges, those that can contribute to the total optical depth, must be made. With the help of criteria similar to those applied in 3.2 based on populations obtained by Abbott (1982, Eq. (8)) it was found that most of the elements with an abundance greater than 1.10^{-5} can be important for the continuum optical depth. Thus the ionization edges of the ground levels from the elements H, He, C, N, O, Ne, Mg, Si and S were considered as contributors to the b-f opacity. Additionally, for the f-f opacity H and He were taken into account and finally Thomson scattering was included. Using this procedure J_ν was evaluated with the continuum source function at 120 frequency points, which are sufficient to ensure an accurate numerical integration of the Eqs. (11). (A tested routine for the solution of the spherical transfer equation using a Feautrier scheme with a Rybicki-type method was kindly provided to the author by J. Puls).

Since the occupation numbers enter Eqs. (6) and (10) and are themselves calculated through the application of these equations, an iteration cycle was needed. After an initial guess for n_i (Abbott's approximation or two-level approximation for strong scattering lines in outer layers) only 7 to 15 iterations were needed until a convergence criterion–relative deviations of 10^{-3}–10^{-4}–was satisfied. Hence, no linearization procedure was required.

For this first step, the continua were kept optically thin. But in the following iterations the continuum radiative transfer was correctly handled. In order to reduce the number of iterations for the He II continuum, this edge was considered as optically thick in the first step–assuming radiative detailed balance–and then iterated until the above convergence criterion was fulfilled. 10 to 15 iterations were needed for the He II continuum and as many when all ionization edges were included.

Another simplifying trick in our rate equation iteration procedure, which saved an enormous amount of computer time must be mentioned. As the occupation numbers vary rather smoothly as a function of the radial distance from the stellar surface and as the radiative bound-bound rates are given by a local approximation, we solve the full set of all rate equations only at 7 radial points chosen from regions with significant velocity, density or optical depth variations. For the continuum radiative transfer a double logarithmic linear interpolation between these radial points is carried out.

At the moment we have still neglected the dielectronic recombination process. We are well aware that even in our cool wind model this can have a non-negligible effect on specific elements. For instance, the calculations of Aldrovandi and Péquignot (1973) indicate that the dielectronic recombination coefficient to C III can be important even at cool temperatures. However, at the moment we are forced to neglect this effect as we need detailed atomic data in order to be able to incorporate it in our detailed calculations. For our rate equations we need the individual transition probabilities of each stabilizing downward transition (see Mihalas and Hummer, 1973). However, only the sum over all these transitions is normally given in the form of a dielectronic recombination coefficient (Nußbaumer and Storey, 1983, 1984, 1986) as required by nebular recombination theory. We therefore have to wait until such data become available to us. However they then could be easily incorporated in our code.

3.4. *Photospheric flux*

At the moment it is still not possible to solve for the photospherical layers with high precision simultaneously together with the envelope of the wind in one "unified" model atmosphere. Hence the emergent fluxes from Kurucz (1979) interpolated to the current effective temperature are used as input for the radiation field longward of 228 Å). Since the model atmospheres of Kurucz include the effect of line-blanketing in a static atmosphere and this has a much greater effect on the emergent flux than the non-LTE treatment without line-blanketing for the effective temperature in question, these models were preferred. Of course, for future work line-blanketed non-LTE fluxes would be desirable, but as is well known the solution of this problem is formidable and is therefore not expected in the very near future.

The application of the Kurucz fluxes involve two additional approximations:

1) neglect of individual photospheric absorption line features–only average continuum fluxes are given;

2) neglect of back reaction from winds on photospheres–"wind blanketing" (see Abbott and Hummer, 1985).

3.5. *Temperature structure*

In the present calculations the local electron temperature was either set equal the effective temperature throughout the wind, or an ad hoc empirical temperature structure appropriate for a gas in radiative equilibrium in NLTE was assumed. In this latter case we followed closely the spherically extended NLTE model atmosphere calculations by Gabler et al. (1986) which take into account the density structure of radiation driven winds but only hydrogen and helium bound-free and free-free opacities.

4. Results

In this section the results of the detailed non-LTE multi-level calculations are presented for two typical O-stars, ζ Pup (O4f)

and τ Sco (O9.5V). These examples have been chosen, since they represent extremes with respect to wind strength, superionization and temperature. In particular, for superionization, τ Sco is a challenge for the theory since it belongs to the latest spectral types where superionization is observed.

4.1. *A wind model for ζ-Pup*

As shown in Paper I, the appropriate choice of stellar parameters is of crucial importance for the solution of the wind dynamics. Fortunately, ζ Pup was subject to two recent detailed non-LTE analyses (Kudritzki et al., 1983, Bohannan et al., 1985) which yielded accurate $T_{\rm eff}$, $\log g$, $R/R_\odot$ and a final model that was able to reproduce not only the observed hydrogen and helium lines, but also a continuous energy distribution that matched well the observed fluxes from the UV to the visual. Accordingly, we adopt the following parameters:

$$T_{\rm eff} = 42{,}000\,\mathrm{K}$$

$$\log g = 3.5$$

$$R_* = 19\,R_\odot$$

In order to test the influence of the different approximations five models were calculated:

Model 1: Calculations of the occupation numbers using Abbott's (1982) approximation (see Sect. 3 and Eq. (12) of this section). The local electron temperature T_e was set $T_e = T_{\rm eff}$ throughout the wind.

Model 2: Correct solution of the full problem as described in Sect. 3. $T_e = T_{\rm eff}$ throughout the wind.

Model 3: Same as model 2, but a slowly falling temperature stratification was adopted (see Fig. 1 and Sect. 3.5).

Model 4: Same as model 2, but with optically thin, geometrical diluted ionizing continua. This means that in Eq. (11) J_ν was replaced by $W B_\nu(T_{\rm rad})$. W is the dilution factor and $T_{\rm rad}$ the monochromatic radiation temperature as obtained from the Kurucz models.

Model 5: Same as model 4 but temperature structure of model 3.

We now discuss the main results of our calculations on the basis of these five models.

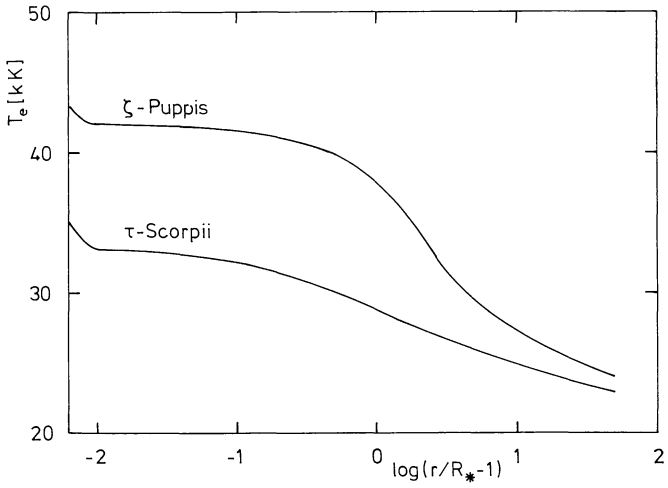

Fig. 1. Temperature stratification for model 3 and 5 of ζ Pup and for the model of τ Sco

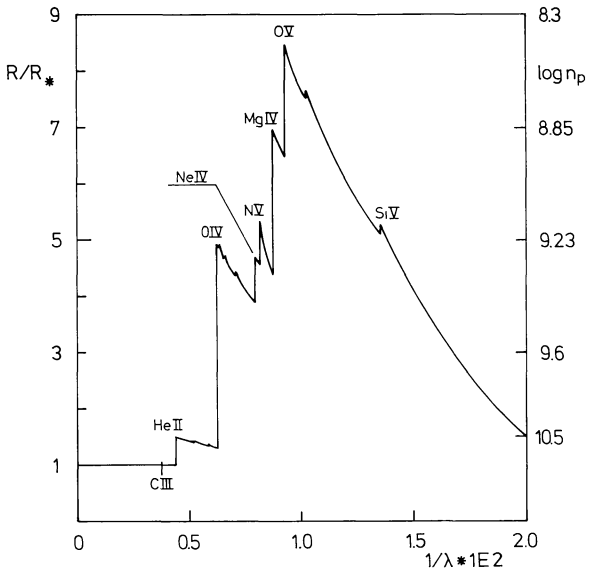

Fig. 2. Radius of continuous optical depth equal unity as a function of reciprocal wave length for model 2 of ζ Pup. On the right ordinate the logarithm of proton density at the corresponding radius is also shown for comparison

4.1.1. Optical thickness of the continuum

Figure 2 shows the radii and density at which the optical depth reaches unity for model 2 as a function of frequency. As was mentioned in Sect. 2, the wind of ζ Pup is optically thick beyond the He II edge. Besides He^+ the main contributors to this thickness are O, Mg, N, Ne and Si. Therefore O-stars with a wind comparable to ζ Pup have an optically thick ionization continuum in the wind even when He is almost fully ionized. The most important consequence of this result is that the ionization balance is mainly determined by the local electron temperature and not by the emergent flux of a static model atmosphere. This is important because hydrostatic model atmospheres produce usually an enormous He^+ absorption edge that strongly underestimates the ionizing radiation field (shortward of 228 Å) in the wind when used as input for ionization calculations.

The optical thickness of the continuum depends on the temperature stratification. For model 3 we obtain a wind which is optically thick shortward of 228 Å throughout the total acceleration region up to 100 stellar radii. The slowly falling temperature (Fig. 1) leads to recombination to He II in the outer parts.

Figure 2 indicates that according to our calculations O V is the strongest ionization stage of oxygen and not O IV as was suggested by Cassinelli and Olson (1979) in their hot corona-cool-wind model calculations. It is therefore questionable if O VI can be produced by the Auger process following the absorption of an X-ray photon. However this will be discussed in more detail below.

4.1.2. Occupation numbers

To be able to discuss our results with respect to the approximations mentioned in Sect. 3 we have to specify the latter. Abbott (1982), Pauldrach et al. (Paper I), Kudritzki et al. (Paper II) adopted an optically thin continuum and optically thick lines for the ionization balance. For the population ratio of ground

states in the ionization stages j and $j+1$ this yields

$$\left(\frac{n_{1,j}}{n_{1,j+1}}\right)_A = \left(\frac{T_R}{T_e}\right)^{1/2} \frac{n_e}{W} \left(\frac{n_{1,j}}{n_{1,j+1} n_e}\right)^*_{T_R} \quad (12)$$

T_R is the photosphere radiation temperature at the frequencies of the continuum transition, W the dilution factor defined by $W = 1/2(1 - \mu_c)$. $\left(\frac{n_{1,j}}{n_{1,j+1} n_e}\right)^*_{T_R}$ denotes the Saha-Boltzmann factor for the temperature T_R. Excited levels were calculated from the Boltzmann formula relative to the ground level in the same ionization stage using T_{eff} ($\approx T_e$) as the relevant temperature.

Abbott and Lucy (1985), however, used a different approach. For the ionization balance they assumed pure recombination theory as in gaseous nebulae. This means that all lines are approximated as being optically thin. This yields

$$\frac{n_{1,j}}{n_{1,j+1}} = \frac{\alpha_T}{\alpha_1} \left(\frac{n_{1,j}}{n_{1,j+1}}\right)_A \quad (13)$$

where α_1 is the fraction of recombinations going directly to the ground state and α_T is the total recombination coefficient including dielectronic recombination. For the excitation of metastable levels they adopted the Boltzmann formula relative to the ground state with T_{eff} as temperature. The excitation of the other levels connected via a single transition to the ground level 1 or a metastable level m is calculated according to (in our nomenclature)

$$\frac{n_i}{n_{1,m}} = \frac{\beta_c}{\beta} \left(\frac{n_i}{n_{1,m}}\right)^*_{T_{R_i}} \quad (14)$$

where $(\mathrm{II})^*_{T_{R_i}}$ is the Boltzmann factor with the photospheric continuum radiation temperature at the frequency of the transition. This equation is derived neglecting stimulated emission and using the assumption that the rate equation of level i is dominated by the radiative rates connecting i with either 1 or m. This latter assumption is of course not correct for lines of large optical thickness because in this case we have β, $\beta_c = 0$ and $J^{1,i}_m = S^{1,i}_m$ (see Eq. (5)) so that the net rate of the transition is zero and cancels from the rate equations even for arbitrary values n^1_m and n_i. In such a situation n_i is determined by other transitions populating or depopulating level i. However, if we have β, $\beta_c > 0$, it must still be shown that other transition mechanisms (for instance electron collisions) are negligible.

In the following we present and discuss our results.

i) Population of ground levels

The stratification of ground level populations for the strongest ionization stages of the elements N, S, Ne, A and Fe for our model 2 are shown in Fig. 3a. To have a direct comparison with Abbott's approximation the results are expressed in units of the numbers obtained by Eq. (12). This means that in Fig. 3a logarithms of the departure coefficients from Abbott's approximation are plotted. As can be seen, *the deviations are considerable and lead to a preference for higher ionization stages.* In the inner part of the envelope they are largest (up to 3.5 dex), whereas they decrease towards the outer part of the wind but still remain significant.

Compared with Abbott and Lucy (1985) the deviations are even larger. We do not demonstrate this with an additional plot since this is immediately evident from Eq. (13) and the fact that $\alpha_T > \alpha_1$ (for examples see Aldrovandi and Péquignot, 1974).

To disentagle whether this is an effect of the optical thick continuum or the multi-level treatment including collisions, we have plotted in Fig. 3b the corresponding results of model 4, where an optically thin continuum is assumed. Obviously, significantly higher populations are also obtained in this case especially in the inner and intermediate part of the envelope. However, in the outer part of the wind the groundstate populations of N V, S VI and A VI decrease rapidly even below Abbott's approximation. This means that the optical thickness of the continuum is the major effect in the outer part of the wind, whereas in the inner part of the wind, where the mass loss rate is fixed, the multi-level treatment dominates. The different behaviour of Ne IV and Fe VI in this region is explained by the influence of metastable levels, which are populated nearly in LTE relative to the ground level in the whole wind, provided that they are not highly excited (see discussion below).

The detailed analysis of the importance of the individual population mechanisms in our rate equations for the important inner part of the wind revealed that–surprisingly–electron collisions

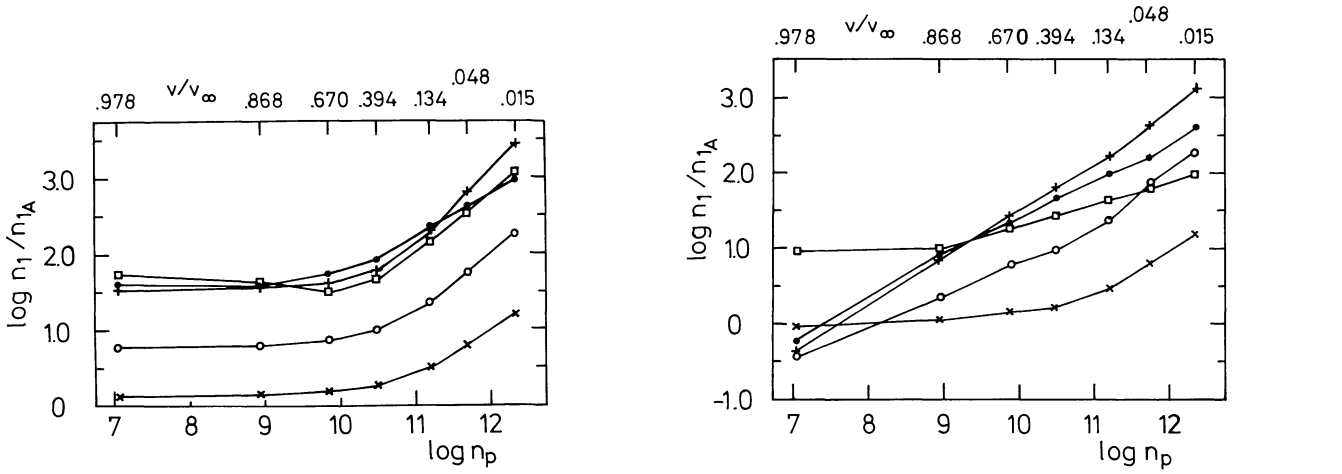

Fig. 3 a and b. The logarithm of the ground state occupation number divided by the value obtained in Abbott's approximation (see Eq. (12)) versus the logarithm of the proton density of ζ Pup: (●) N V, (○) S VI, (×) Ne IV, (+) A VI, (□) Fe VI. For a detailed discussion see text. **a** model 2, **b** model 4 (the calculations are based on the hydrodynamical structure of model 3)

are dominant for the excitation of lower lying levels above the ground state. This is caused by the fact that most of the lines of the relevant ions have escape probabilities β, β_c very close to zero, so that their net rates are unimportant (This concerns mainly the principal ionization stages of each element, which produce the strongest lines.). Moreover, it turns out that for an individual excited level the collision rates dominate also over radiative ionization and recombination rates at least up to levels that have ionization edges with $\lambda_{\text{Ion}} < 300$ Å (for a more detailed estimate see Appendix C). The result is that such lower lying excited levels have populations very close to LTE relative to their ground state (this holds especially for metastable levels, see also iii):

$$\frac{n_i}{n_1} \approx \left(\frac{n_i}{n_1}\right)^*_{T_e}, \quad \text{for } i \leq i_{\max}. \tag{15}$$

Since Eq. (15) is identical for the population of excited levels with the one used in Abbott's approximation, it is of course at first glance surprising as to why we obtain such large deviations in Fig. 3b. The answer is, however, simple and lies in the treatment of total ionization and recombination.

While Abbott allows for ionization and recombination from and towards the ground level only, our multi-level calculations include the same processes from excited levels as well. Consequently, in the Abbott-approximation the ionization equation is

$$n_1 R_{1k}(T_R) = n_k R_{k1}(T_e), \tag{16}$$

where the radiative rates are defined by Eq. (11) (for $J_\nu = W B_\nu(T_R)$ and stimulated emission neglected this is equivalent to Eq. (12)). In an analytically simplification of our case (model 4), however, a "block of LTE-populated levels" contributes to radiative ionization and recombination:

$$n_1 \sum_{j=1}^{i_{\max}} (n_j/n_1)^*_{T_e} R_{jk}(T_R) = n_k \sum_{j=1}^{i_{\max}} R_{kj}(T_e). \tag{17}$$

(It can be shown easily that collisional ionization and recombination are unimportant in this cool wind model). Now it is important to realize that $R_{jk}(T_R) \propto \exp(-h\nu_{jk}/kT_{R_j})$ and that T_R ($\lambda < 228$ Å) $\approx 30{,}000$ K (see Kurucz, 1979), whereas T_R ($\lambda > 228$ Å) $\approx T_{\text{eff}} = T_e$. This means that the ionization probability from excited levels with $\lambda_j > 228$ Å is much larger than from the ground state. If one reduces the sum on the left side of Eq. (17) to $\sum_{l \in M} (n_l/n_1)^* R_{lk}(T_R)$ with l being the lowest level for which $\lambda_l > 228$ Å and $\lambda_{l_1} \approx \lambda_{l_2}$ for $l_1, l_2 \in M$, one obtains a lower limit for the ionization departure coefficient

$$\left(\frac{n_k}{n_1}\right) \Big/ \left(\frac{n_k}{n_1}\right)_A > \sum_{l \in M} \frac{(n_l/n_1)^*_{T_e} R_{lk}(T_{R_l})}{R_{1k}(T_{R_1})} \frac{R_{k1}(T_e)}{\sum_j R_{kj}(T_e)} \approx \frac{\alpha_1}{\alpha_T} \frac{T_e}{T_{R_1}} \frac{v_l^2}{v_1^2}$$

$$\exp(-h\nu_1/kT_e) \exp(h\nu_1/kT_{R_1}) \sum_{l \in M} g_l/g_1 \gg 1, \tag{18}$$

where the photoionization cross sections at threshold were assumed to be equal.

Table 1 gives values calculated according to Eq. (18) and the corresponding correct calculated values of model 4 (inner part of the wind) for the ions displayed in Fig. 3. The comparison shows (see also Fig. 3b) that Eq. (18) gives a reasonable order of magnitude estimate, at least for the inner part of the envelope where the lines have still a very small escape probability. The gradient in Fig. 3b, which is not predicted by Eq. (18) occurs because the collisional rates decrease and the escape probabilities increase outwards, which leads to a depopulation of upper levels and consequently weakens the ionization from excited levels. This is discussed in more detail in the following subsection.

Table 1

Upper ionization stage (n_k)	Excitation energy (l) (10^5 cm^{-1})	$\text{Log}(n_k/n_{k_A})$	
		Approximate value (Eq. 18)	Correct value (model 4)
Ne IV	2.046	1.16	1.20
N V	2.354	2.60	2.63
S VI	2.000	2.15	2.30
A VI	2.186	3.36	3.13
Fe VI	2.213	2.43	2.00

ii) Population of radiatively coupled low lying levels

We have shown that for low lying levels n_i/n_1 corresponds to the LTE value if the radiative b-b rates are in detailed balance. Thus lines in the optically thick limit do not influence the populations if electron collisions are strong enough and lines in the optically thin limit depopulate the occupation numbers relative to the LTE value (see the discussion of Eq. (14)). Hence, the question arises up to what point in the wind even the strongest lines can be so optically thick that the corresponding rates are in detailed balance. The corresponding departure coefficients defined as $(n_i/n_1)/(n_i/n_1)^*$ for the upper levels of the resonance lines of C IV and N V are given in Fig. 4. Both lines are in clear detailed balance up to a particle density of 10^{11}. Therefore, the population of the upper level of the C IV and N V resonance lines are determined by collisions in the lower and approximately in the intermediate part of the wind. In the upper part of the wind the line radiation field dominates and pure resonance scattering dominates the population of the upper level.

iii) Metastable levels and connected high lying excited levels

Metastable levels are of special interest for the wind acceleration mechanism since their radiative decays are strictly forbidden

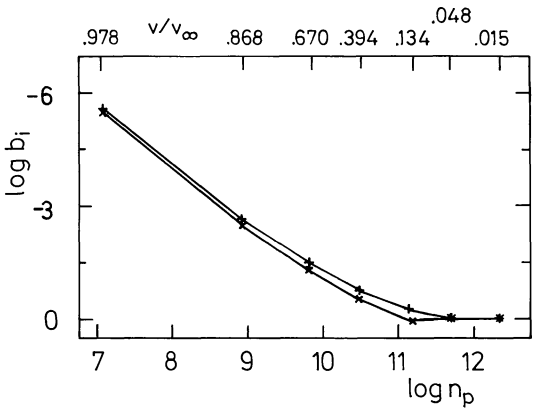

Fig. 4. Logarithmic departure coefficients for the upper levels of the resonance lines of C IV (+) and N V (×) as a function of logarithmic proton density. Note the definition of $b_i = (n_i/n_1)/(n_i/n_1)^*$ (see also text)

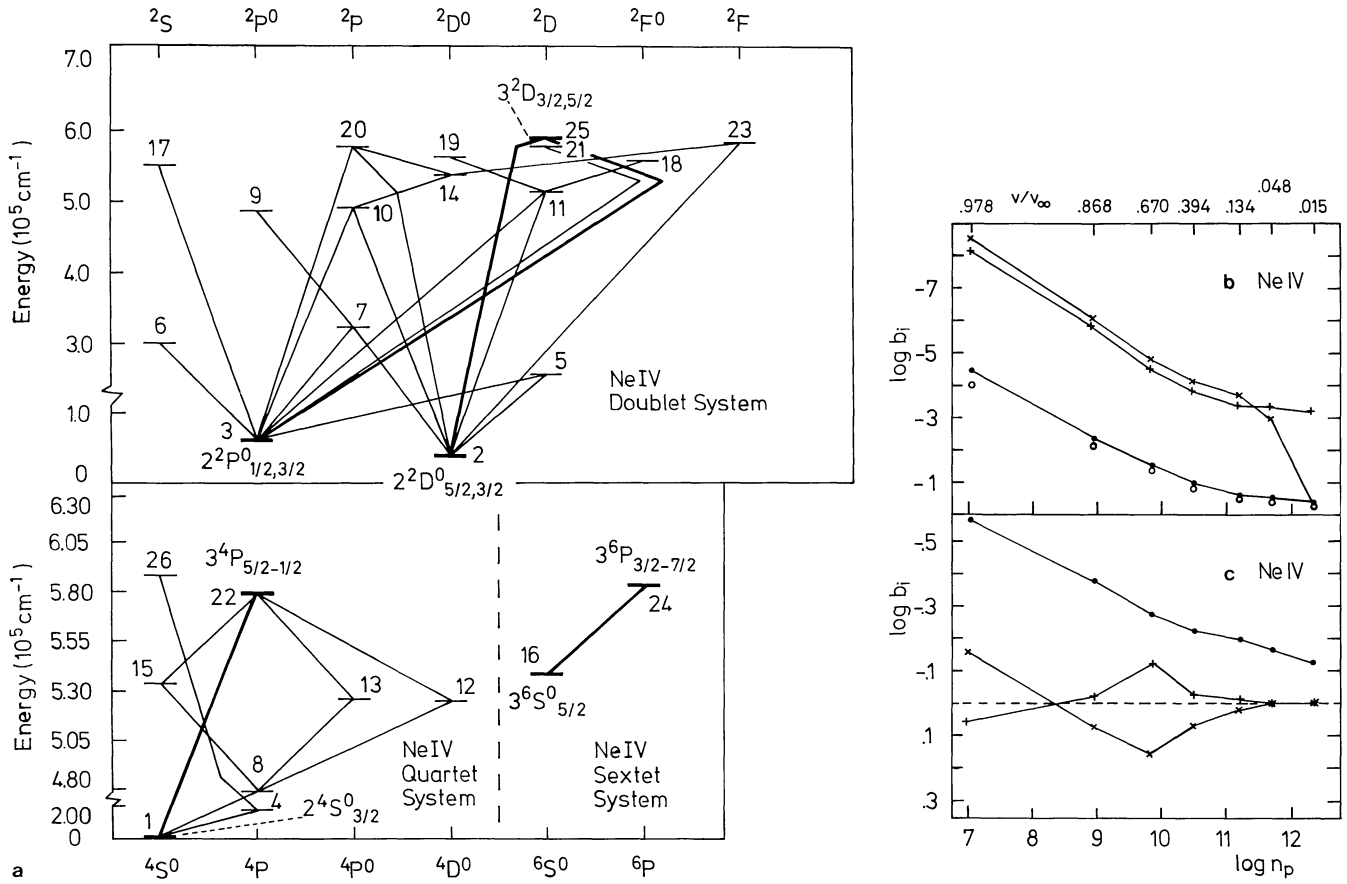

Fig. 5. **a** Simplified Grotrian diagram of Ne IV. **b** Logarithmic departure coefficients for the three excited levels of Ne IV marked in Fig. 5a: (+) $3^2D_{3/2,5/2}$, (×) $3^4P_{5/2-1/2}$, (●) $3^6P_{3/2-7/2}$. **c** Same as Fig. 5b for the three metastable levels (x) $2^2P^0_{1/2,3/2}$, (+) $2^2D^0_{5/2,3/2}$, (●) $3^6S^0_{5/2}$

under wind conditions. Consequently, they are strongly populated and thus these levels contribute to the total photoionization rate throughout the wind and the related lines contribute strongly to the line force. Therefore we discuss as an example the three metastable levels of Ne IV together with three high lying, radiatively coupled excited levels. A simplified Grotrian diagram with the corresponding levels (note that the population of the ground state ($2^4S^0_{3/2}$) has already been discussed in i) is given in Fig. 5a.

The departure coefficients (defined as in ii) of the metastable levels ($3^6S^0_{5/2}, 2^2D^0_{5/2,3/2}, 2^2P^0_{1/2,3/2}$) are displayed in Fig. 5c, whereas in Fig. 5b the departure coefficients of the excited levels are plotted ($3^6P_{3/2-7/2}, 3^2D_{3/2,5/2}, 3^4P_{5/2-1/2}$). Also given in Fig. 5b is the dilution factor (open circles). These values should be approached for excited levels coupled by an optical thin line (see discussion of Eq. (14)). This is well reproduced for the excited level of the sextet system because it is only radiatively coupled to the metastable level by a line that is in the optically thin limit throughout the envelope. However, the lower metastable level of this line, for which Abbott (1982) and Abbott and Lucy (1985) assumed LTE, deviates from LTE as it is determined mainly by collisions in the inner part and by b-f processes in the outer part of the envelope (see i).

Another interesting case is the population of the excited quartet level which is radiatively coupled to the ground state. The corresponding line is optically thick throughout the wind ($T_R \approx T_e$). However, apart from the innermost part of the wind ($n_p \approx 10^{12}$) the line rates are not in detailed balance, since the collision rates are too weak due to the high excitation energy of the level. Thus, the approximation made by Abbott and Lucy (see Eq. (14)) is nearly correct for high lying excited levels.

A more complicated case are the levels of the doublet system since they represent a real multi-level situation. As the metastable levels are low lying levels they are in LTE as long as their influencing lines are in the optically thick limit. But this holds strictly only up to a particle density of 10^{11}. Below this density the lines gradually deviate from detailed balance. If the gf-values belonging to the $2^2P^0_{1/2,3/2}$ level are greater or lower than those belonging to the $2^2D^0_{5/2,3/2}$ level, the electrons are reshuffled due to lines with equal upper levels. This process, which explains the departures of the doublet metastable levels shown in Fig. 5c, does not work for lines which become optically thin.

4.1.3. Superionization

As discussed in Sects. 1 and 2 the observations show in the wind of ζ Pup the existence of anomalous high stages of ionization like O VI together with low stages like C III. If our models are basically correct, they should be able to reproduce the observed resonance lines of O VI and C III at least qualitatively. As far as O VI is concerned, we are encouraged by the results of Sect. 4.1.2.i). A simple estimate using the approximation of Eq. (18) yields $\log(n_{O\,V}/n_{O\,V,\,Abbott}) \approx 3.14$ (the correctly calculated value

of model 4 (inner part of the wind) is 3.20) and $\log(n_{\mathrm{O\,VI}}/n_{\mathrm{O\,VI,\,Abbott}}) \approx 7.32$ (the correctly calculated value of model 4 is given in Fig. 6a).

Figure 6 shows the results of the calculations for the different models together with the observed ionization fractions. We first discuss O VI (Fig. 6a). As was to be expected from our estimate, model 1 (which makes use of the Abbott-approximation) fails completely. However model 4, in which an optically thin continuum is still adopted but where collisons are included in the multi-level calculation, comes much closer to the observations in the lower and intermediate part of the wind, whereas in the outer part no improvement is achieved. Therefore, the effect of ionization from collisionally excited levels alone is not sufficient to produce observable O VI. Including, however, the effect of the optically thick continuum (model 2) leads to an additional increase, especially in the outer part of the wind, and to rough agreement with the observed value.

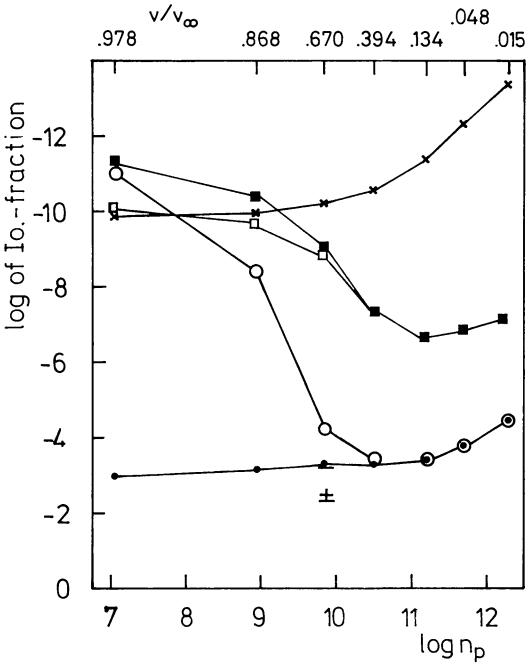

Fig. 6a. Logarithmic ionization fraction of O VI for the 5 models of ζ Puppis: (×) model 1, (●) model 2, (○) model 3, (■) model 4, (□) model 5. The cross corresponds to the observed value determined by Lamers and Morton (1976) and the two nearby bars to the limits found by Hamann (1980), (the calculations are based on the hydrodynamical structure of model 3)

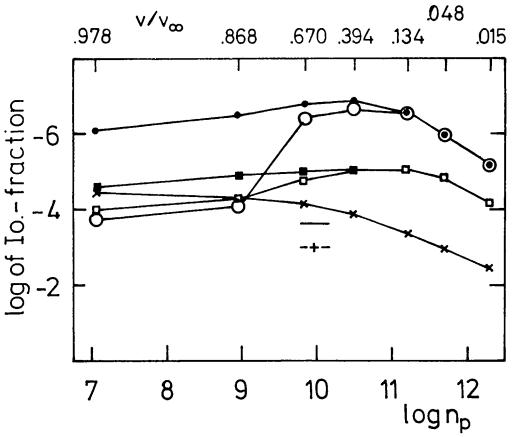

Fig. 6b. Same as Fig. 6a, but for C III

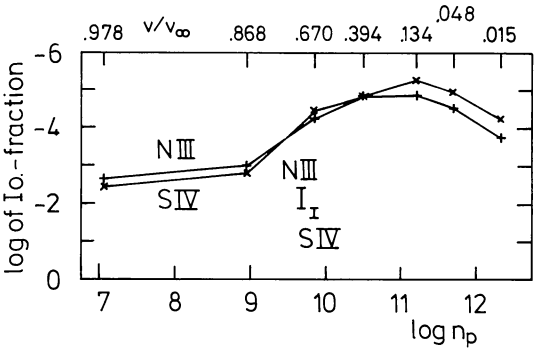

Fig. 6c. Ionization fractions for model 3 of ζ Pup for S IV (×), N III (+)

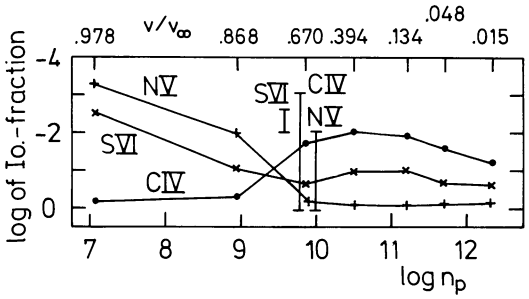

Fig. 6d. Same as Fig. 6c, but for S VI (×), N V (+), C IV (●). (The vertical bars correspond to the observed values, Lamers and Morton, 1976; Hamann, 1980)

On the other hand, we also have to explain C III. As Fig. 6b shows, model 1 (Abbott's-approximation) is much closer to the observations than multi-level models 4 and 2, which of course again lead to much higher ionization. Consequently, a hasty conclusion would be that our "improved" NLTE calculations now solve the superionization problem but fail to reproduce low ionization stages like C III. However, the results for model 3 and 5 (temperature stratification with correct and optically thin continua, respectively) indicate that this is not the case. Due to the temperature stratification we obtain O VI in the inner and intermediate part of the wind and C III in the outer layers. Line profiles calculated with the occupation numbers of model 3 are given in Fig. 7 (for the red doublet components only to give a qualitative impression. A detailed comparison with observations will be given in a follow-up paper. The profile calculations were made using the same program as described in Paper I, which was kindly made available by J. Puls). The results are in rough agreement with the observations. Observable O VI is clearly produced by our calculations, although v_∞ is not fully achieved in the profile. C III is obtained only between $0 \leq v/v_\infty \leq 0.15$ and $0.7 \leq v/v_\infty \leq 1$ in the moment. However, we feel that further improvements (dielectronic recombination for C III (see 3.3.), modified temperature structure for O VI) will allow to overcome these problems.

Additionally, Fig. 6c and 6d show for model 3 the ionization fractions of S IV, N III and S VI, N V, C IV, respectively. The comparison with the observed fractions (Hamann, 1980; Lamers and Morton, 1976) are within the same quality as for O VI and C III.

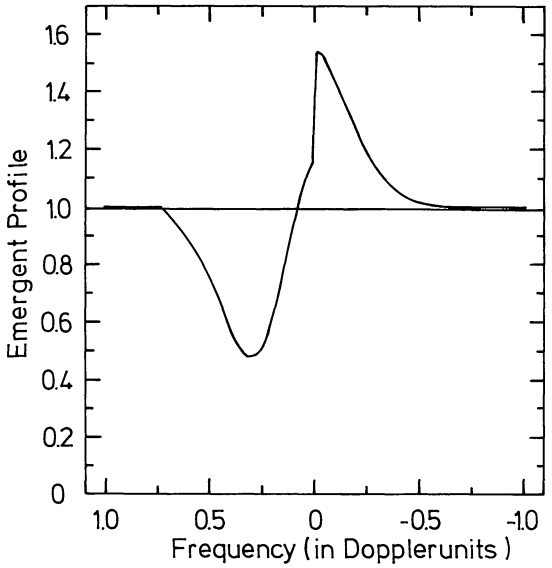

Fig. 7a. Profile of the red doublet component of the O VI resonance line computed for model 3 of ζ Pup

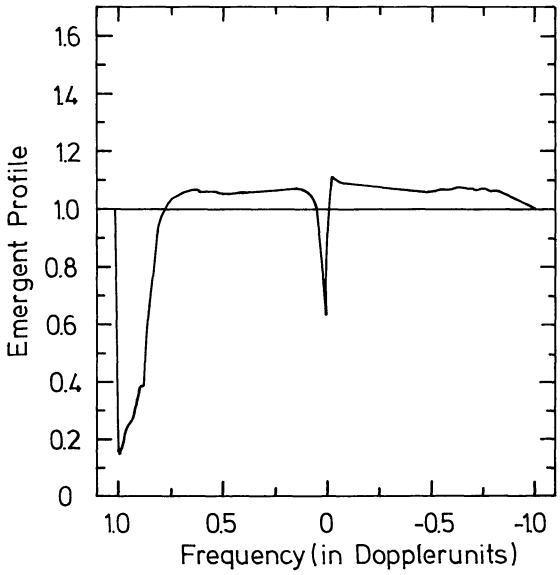

Fig. 7b. Same as Fig. 7a, but for the C III resonance line

We thus conclude that a cool wind model with a detailed self-consistent non-LTE multi-level treatment for the populations is able to reproduce the principle behaviour found by observations.

4.1.4. Back reaction on line force and wind dynamics

Now we discuss the back reaction of the level population changes on the line force and the wind dynamics. The force multiplier $M(t)$ (the total line force in units of the Thomson-scattering force, $t = \sigma_e \rho v_{th}/v'$ the wind depth variable, see Paper I or Abbott, 1982) is shown in Fig. 8 for four of our models. Obviously, there are great differences between model 1 and the other models 2, 3, 4 based on the non-LTE multi-level calculations. The reason for this is, of course, the change in ionization balance as discussed in Sects. 4.1.2 and 4.1.3. Since the higher ionization stages

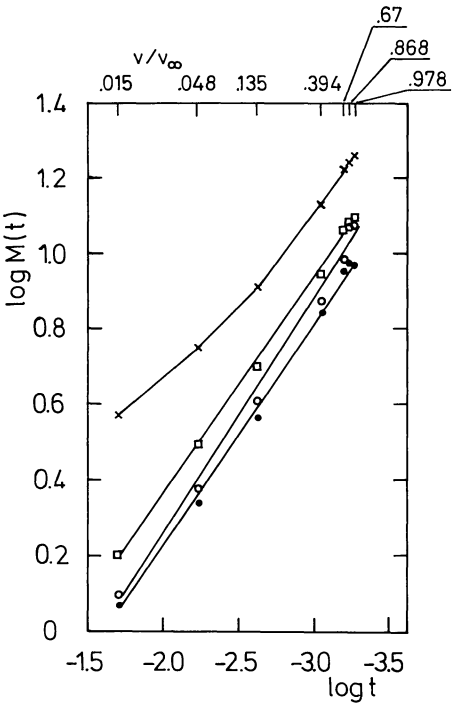

Fig. 8. Logarithm of the force multiplier as a function of depth parameter t (for definition see text) for four models of ζ Pup. (×) model 1, (●) model 2, (○) model 3, (□) model 4. (The calculations are based on the hydrodynamical structure of model 3)

have fewer strong lines at the radiative flux maximum, the net radiative line force decreases for models 2, 3 and 4.

In addition to the total line force it is also interesting to discuss how much of the acceleration is provided by lines in the optically thick limit and which individual elements are providing the line force.

The percentage contribution of lines in the optically thick limit for the models 1, 2, 3, 4 are given in Fig. 9. The most significant feature, in the lower and intermediate part of the wind, is the large contribution of optically thick lines in the non-LTE models with the correctly calculated continuum (models 2 and 3).

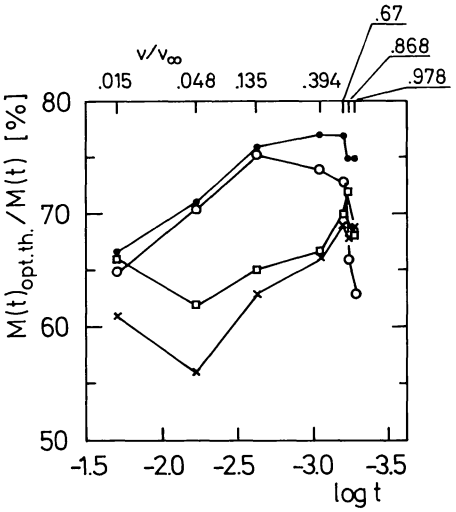

Fig. 9. Same as Fig. 8 for the fractional contribution of strong lines to the force multiplier

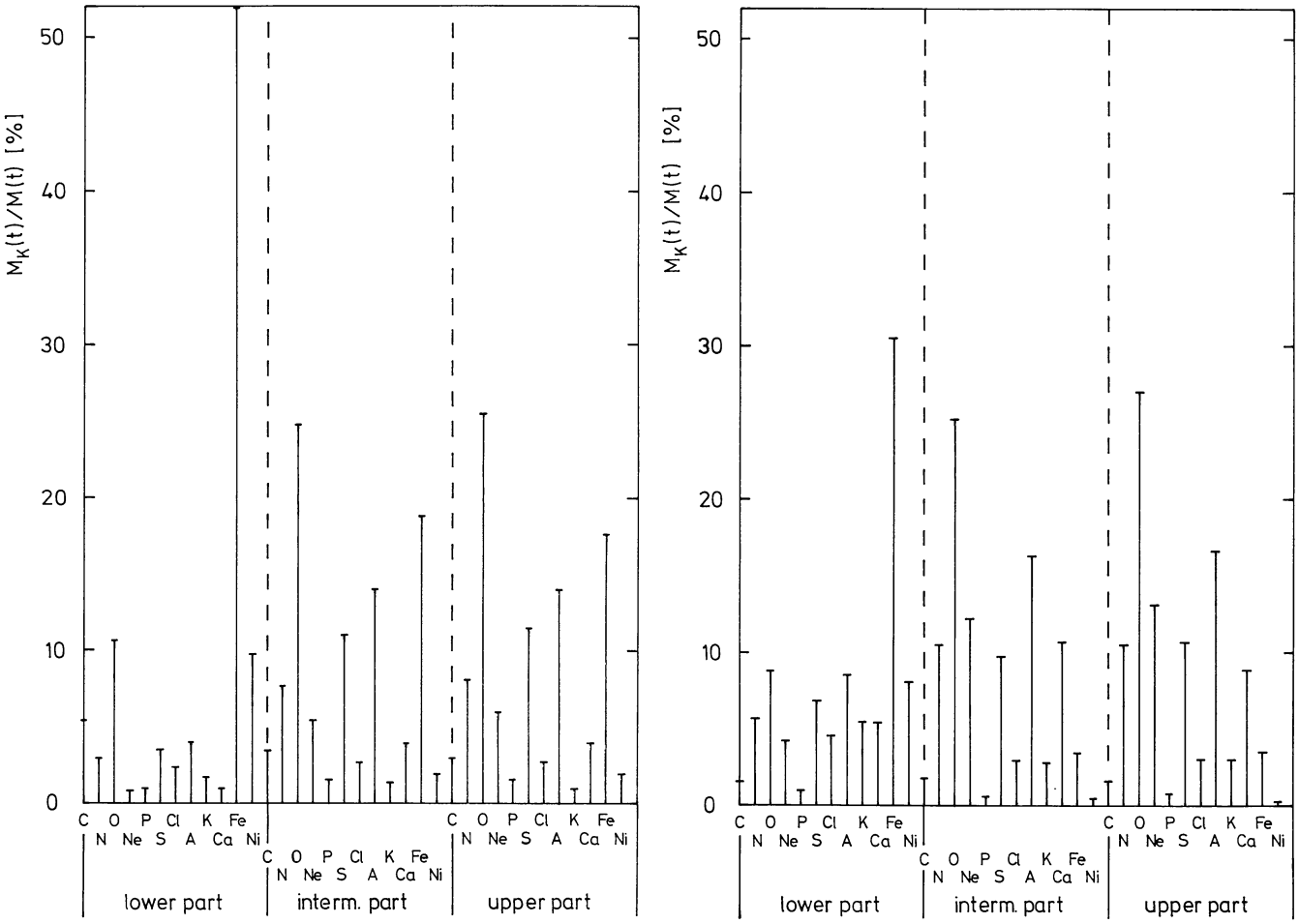

Fig. 10a and b. Individual contribution of the most important elements to the line force at inner, intermediate and outer part of the wind. **a** model 1; **b** model 2. (The calculations are based on the hydrodynamical structure of model 3)

Here up to 75% of the force comes from lines in the optically thick limit. In the outermost part of the envelope the contribution of thin lines increases in all models as a consequence of the lower density.

Figure 10 shows the distribution of the line force on the most important elements for a point in the lower, intermediate and upper part of the wind, respectively. Iron, oxygen, sulphur and argon are the main contributors in model 1 (Fig. 10a), whereas the influence of iron is strongly reduced in model 2 (Fig. 10b) and Ne, N and Ca are much enhanced. However, no single element dominates the acceleration throughout the envelope in either of these models.

An additional important question is, which ionization stages of an element contribute most to the force? As an example, Fig. 11 shows the distribution of the force on the important ionization stages of iron for models 1, 2, 5. The striking feature of Fig. 11 is that Fe IV contributes less to the force for model 5 and even less for model 2 than model 1. The opposite holds for Fe VI. This shift to higher ionization stages of Fe is mainly responsible for the decrease of the total line force in the non-LTE models and has important consequences for the mass-loss rate that is significantly reduced by this effect.

The results of our hydrodynamical radiation driven wind calculations (see Sect. 3) are summarized in Table 2. It is very satis-

Table 2. Wind parameters

Model	1	2	3	4	5	Observation	Source
$\dot{M}$ $(10^{-6} M_\odot\,\mathrm{yr}^{-1})$	14.	4.5	4.6	8.0	8.3	4 to 6	a
v_∞ $(\mathrm{km\,s}^{-1})$	1600.	1920.	2200.	1687.	1565.	2450. 2660.	b c

a) Abbott and Lucy (1985)
b) Hamann (1980)
c) Lamers and Morton (1976)

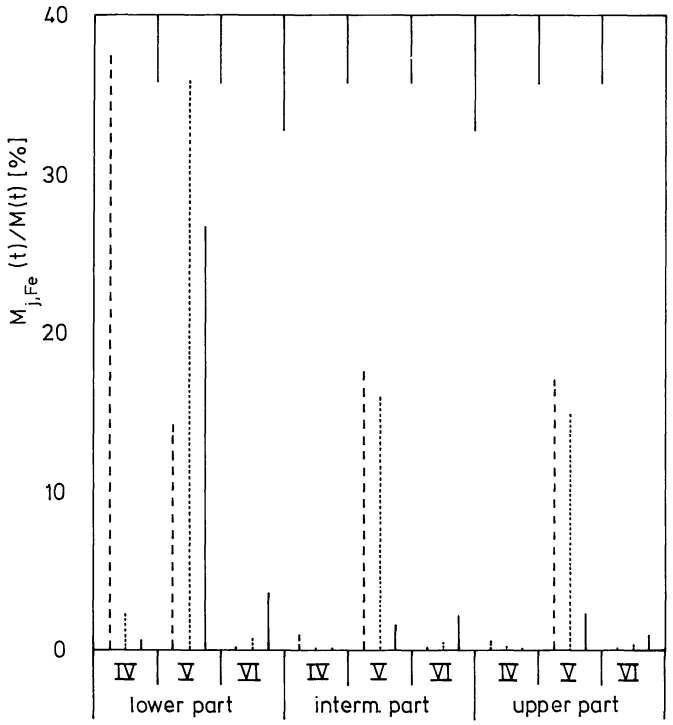

Fig. 11. Distribution of the line force contribution of the ionization stages of Fe for model 1 (dashed), model 2 (fully drawn), model 5 (dotted) of ζ Pup at three depths in the wind. (The calculations are based on the hydrodynamical structure of model 3)

fying to see that, while model 1 (with the most simplified approximations for the occupation numbers) fails to reproduce the observations in a quantitative sense, model 3 (the most elaborate one) comes very close. Only a few hundred km s^{-1} are lacking for v_∞. However we believe that with the inclusion of the effects of line overlap this difference will vanish.

A brief comment is necessary on Paper I. Here Pauldrach et al. on the basis of calculations as in model 1 achieved good agreement with the observed values of $\dot{M}$ and v_∞. As model 1 now fails in the case of ζ Pup the question arises as to why these calculations did not fail for the objects in Paper I. The answer is simple. As the stellar parameters of the objects in Paper I taken from literature were not very precisely determined, they were "adjusted in an allowed range" to demonstrate that the improvements made in Paper I allowed the observations to be matched in principle. It was, however, pointed out that a very detailed comparison with objects with precisely determined parameters via detailed spectroscopic NLTE analyses would be necessary to provide a real test of the theory. ζ Puppis is such an object in which one cannot "adjust", for instance, $\log g$ by more than ± 0.1 dex. It is therefore very important that the much more sophisticated (and extensive) calculations come closer to the observations.

4.2. A wind model for τ-Sco

The most accurate determination of the effective temperature and gravity has been made recently by Herrero (1986), who used a non-LTE model in order to compare the observed hydrogen and helium spectrum with numerical predictions. The derived values are:

$T_{\rm eff} = 33{,}000$ K, $\quad \log g = 4.15 \pm 0.1$

A problem for the present purpose is the great uncertainty in the stellar radius. Lamers and Rogerson (1978) found a value of $R = 6.7\,R_\odot$ using an absolute V-magnitude derived from the β-index and the predicted bolometric correction. On the other hand, using the distance of $d = 178. \pm 10$ pc obtained from the motion of the Scorpius-Centaurus association (Bertiau, 1958) the model atmosphere flux and the apparent dereddened V-magnitude, a value of $R = 5.5\,R_\odot$ is derived (Kudritzki, private communication). Finally with $d = 62.5^{+62.5}_{-21.}$ pc as obtained from trigonometric parallaxes (Jenkins, 1951) $R = 3.5\,R_\odot$ is found.

A comparison of the radii with evolutionary models suggests a somewhat evolved main sequence star for the first radius, a ZAMS-star for the second and a hot subdwarf-O-star for the third one. (Of course, it seems to be adventurous to consider τ Sco as a hot subdwarf-O-star and thus we shall ignore the last radius). In the present calculations a radius of $5.5\,R_\odot$ is adopted.

A slight modification is made concerning the element abundances. Contrary to ζ Pup, only a few elements contribute to the line force (see below). Taking into account the results of Hardorp and Scholz (1969), Schönberner et al. (1986), Gehren et al. (1985) a reduction by a factor of 1.5 was adopted for these elements.

As for ζ Pup a slow falling temperature structure for radiative equilibrium was assumed (see Fig. 1). Thus, the following model corresponds to model 3 of ζ Pup.

As the wind density of τ Sco is much smaller than that for ζ Pup (2 dex in density at comparable radii (r/R), see below), the total continuum is optically thin in the whole wind. Thus the continuous mean intensity that enters in the photoionization and recombination rates is formed mainly at the base of the wind at a local electron temperature of 30–35 kK (note: this leads to a much higher radiation temperature than is given by Kurucz, 1979). For ζ Pup we have shown that it is possible to explain the observed high ionization species by photoionization from all considered levels in a cool wind model. As τ Sco has a significantly smaller effective temperature, it is a priori questionable whether the anomalously high ionization stages, observed also for τ Sco, can be explained by the same mechanism. Figure 6a (model 3 of ζ Pup) indicates that for a local temperature of 33 kK ($v/v_\infty \approx 0.868$) the O VI ratio is smaller than the observed one for τ Sco (see Hamann, 1981; Lamers and Rogerson, 1978). However, as shown by the same authors, the mass loss rate for τ Sco is approximately 3 dex smaller than for ζ Pup. Adopting nearly the same velocity law for both stars yields a 2 orders of magnitude decrease in the density at equivalent depths. Consequently the radiative recombination coefficients, which are linearly proportional to the density, decrease markedly. Additionally, the radiation temperatures of the line-blanketed photospherical emergent fluxes are greater than $T_{\rm eff}$ for some threshold values of excited O IV, O V and N IV, N V levels and these levels contribute an important amount to the total photoionization rate of each ionization stage (see 4.1. 2.i), as in the case of τ Sco are less lines in the optically thick limit (see below) and collision rates are smaller due to the decreased density, mainly metastable levels are affected). Thus, no easy estimate for the superionization is possible. Only a detailed calculation can give an answer.

The force multiplier $M(t)$ for τ Sco is shown in Fig. 12a. Compared with ζ Pup (see Fig. 8) a completely different structure for the force multiplier is obtained. Thus, it is not surprising that the character of the individual lines that contribute to the acceleration has also changed. Figure 12b shows the percentage

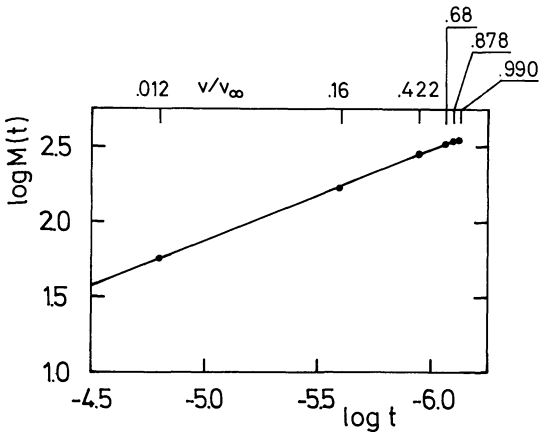

Fig. 12a. Logarithmic line force multiplier for the τ Sco model

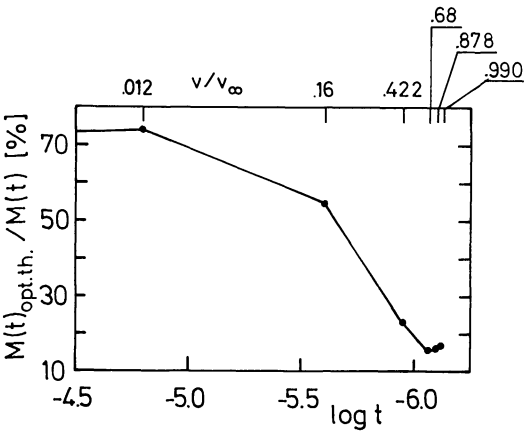

Fig. 12b. Fraction contributed to the force multiplier by strong lines

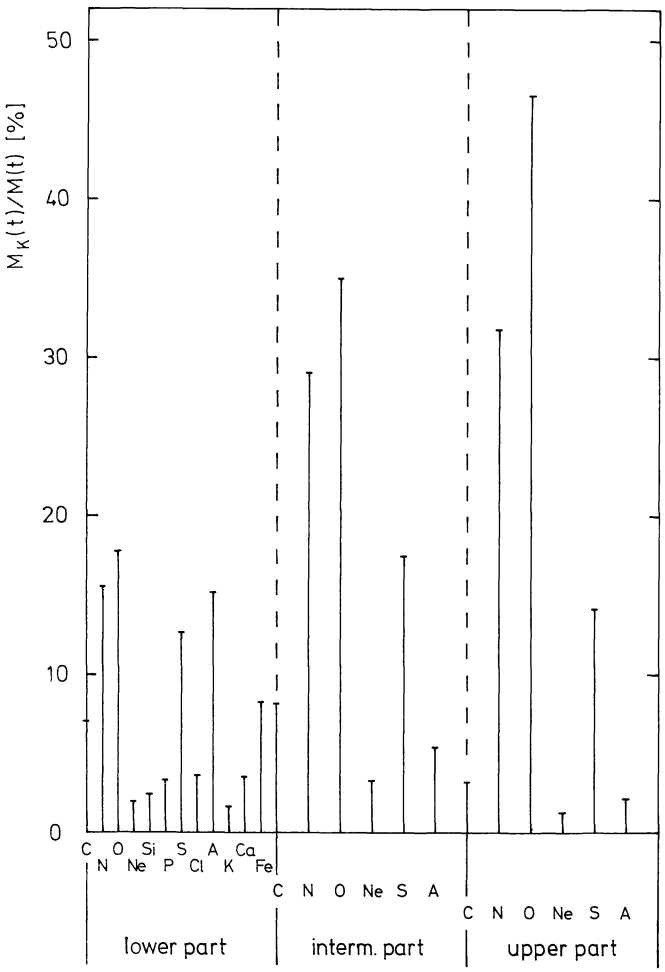

Fig. 13. Elemental distribution of the line force in the lower, intermediate and upper part of the wind model of τ Sco

contribution of lines in the optically thick limit. The striking feature is that optically thick lines contribute more than 50% to the total line force only up to $v = 0.2v_\infty$. In the outer layers this contribution is reduced to 15%. Thus in the intermediate and outer part of the envelope the wind is driven mainly by lines that are not opaque enough to have observable, blue-shifted, absorption profiles. Because of this, it is questionable as to whether this part of the halo can be really observed in P Cygni profiles. Another interesting point concerns the distribution of the individual elements on the force multiplier. Figure 13 shows that at the base of the envelope the force is distributed among many elements, as usual. But in the intermediate and outer part of the halo only O, N, Ne, C, A and S contribute to the force, the amount from all other elements is negligible. This indicates that only this small number of elements are relevant for the low dense wind of τ Sco.

The mass loss rate derived for the applied model is $\dot{M} = 5.10^{-9} M_\odot \,\mathrm{yr}^{-1}$. A value that is close to the empirically estimated ones of Lamers and Rogerson (1978) $\dot{M} = 7. \pm 1.6\,10^{-9}$ $M_\odot \,\mathrm{yr}^{-1}$ and Hamann (1981) $\dot{M} = 2. \pm 2.10^{-9} M_\odot \,\mathrm{yr}^{-1}$. For the terminal velocity the obtained value is, with $v_\infty = 3850$ $\mathrm{km\,s}^{-1}$, much greater than $v_\infty \approx 2000\,\mathrm{km\,s}^{-1}$ derived from absorption profiles (see Hamann; Lamers and Rogerson). But, as was suggested above, it seems that the dynamically obtained terminal velocity cannot be derived from absorption profiles due to the low density far out in the wind (see below). This is also supported by the extremely large acceleration of the flow (see Fig. 14) which gives $v \approx 2000\,\mathrm{km\,s}^{-1}$ at $R = 2.\ R_*$ – also suggested by Lamers and Rogerson – and which ensures that the observed envelope is close to the star.

In Fig. 15 the observed (Hamann, 1981) and calculated ionization ratios of C IV, N V, and O VI are compared. The calcula-

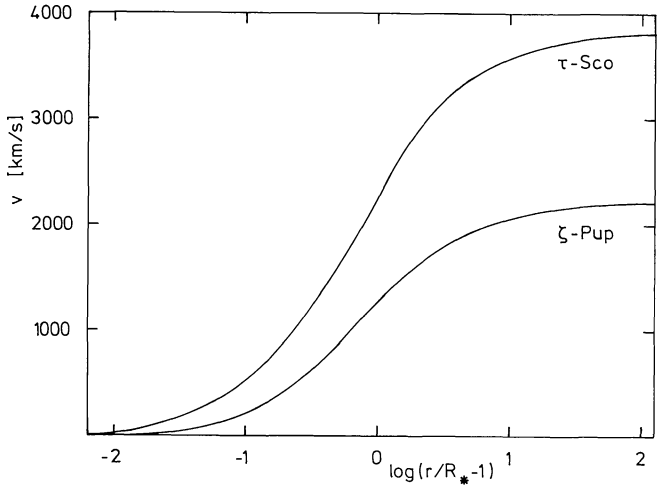

Fig. 14. The theoretical velocity fields for ζ Pup and τ Sco

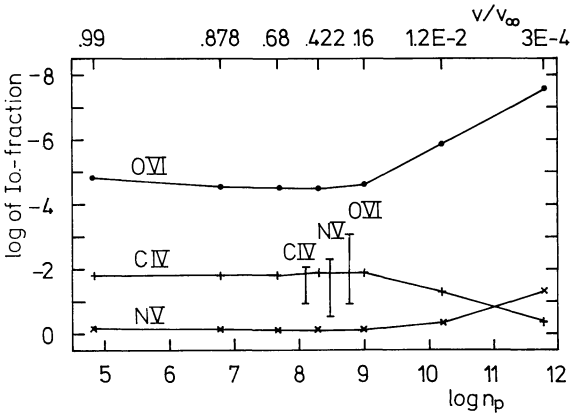

Fig. 15. Calculated ionization fractions of O VI (●), N V (×) and C IV (+) for the τ Sco model

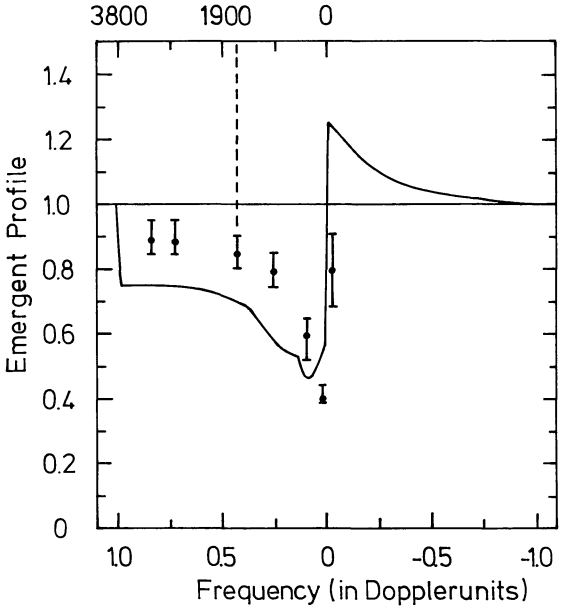

Fig. 16. Comparison between the observed and calculated blue component of the N V doublet resonance line for the τ Sco model. The bars indicate the location of the observed values (see Lamers and Rogerson, 1978). These are somewhat below the assumed continuum even for velocities up to 3000 km s^{-1}). The dashed line represents the terminal velocity assumed by Lamers and Rogerson for the N V line. For a detailed discussion see text

tions give the observationally suggested ratio of C IV and for N V a value only 0.5 dex larger than the observed one, but at least 1 dex is missing for O VI. Nevertheless it is not yet possible to decide if this difference can be decreased through a more elaborate calculation of the ionization balance. We have had to make a variety of approximations for the atomic data (see Appendix). In addition, as pointed out in Sect. 4.1.2.i), the ionization balance depends *crucially on the emergent photospheric flux* due to photoionization of excited levels. At the moment we feel that a calculation in which no use of an emergent photospheric flux is made, but rather the envelope and photosphere are treated fully consistently, can decrease the "small" deviation of 1 dex for the O VI ratio. The increase in photoionization from excited levels in the lower part of the wind also explains the decrease in the high ionization species in the outer part of the envelope (see Lamers and Rogerson). Since in the outer part, the ionization equilibrium drops to lower stages when the lines become optically thin (see Sect. 4.1.2.i), the photoionization from excited levels is of less importance. Additionally, dielectronic recombination has a non negligible influence in this region due to the extremely low density.

In Fig. 16 the N V doublet line profile is given. For this calculation the doublet was considered as a single line since only a qualitative comparison with observations is intended at the moment. The basic features of Fig. 16 are:

– The emission component is about 20% above the continuum. This is in agreement with observations (Lamers and Rogerson found about 10%).

– As N V already exists at the base of the envelope (see Fig. 15) the strongest absorption occurs at a very low velocity $v \approx 200$ km s^{-1}. This result is also consistent with observations.

– For velocities greater than 1600–2000 km s^{-1} the absorption wing drops to almost 80% of the continuum level. As the observed far blue wings for N V, O VI and C IV also lie immediately below the continuum level in this velocity range, this confirms our conclusion about the ionization stratification and the fact that absorption features with $v > 2000$ km s^{-1} are scarcely detectable. Consequently, v_∞ might be much larger, as predicted by the absorption lines.

5. Conclusions and future work

By our calculations we have demonstrated that non-LTE multi-level effects are extremely important for the ionization and excitation in the plasma of hot star stellar winds. Previous approximations such as the "quasi-gaseous nebula approximation" used by Abbott (1982), Pauldrach et al. (1986), Kudritzki et al. (1986) and the complete gaseous nebula approach by Abbott and Lucy (1985) do not lead to a quantitatively correct description of the ionization fractions in cool wind models. As a result of our improvements, a signficant shift to higher ionization stages is found. This is caused by the correct radiative transfer of the optically thick continuum shortward of 228 Å. This effect is enhanced by collisional excitation of low lying excited levels with ionization wavelengths larger than 228 Å and subsequent photoionization from these levels that are exposed to the full photospheric continuous radiation field.

Excited levels – in particular those with very strong resonance line transitions – are in many cases poorly approximated by the collision free two-level approximation at least up to $n_e \geq 10^{10}$ cm^{-3}. The reason is that the net rates of these transitions cancel from the rate equations because of their large optical thickness. Consequently, the corresponding occupation numbers are determined by the remaining transitions, i.e. collisions, bound-free rates and other line transitions. The consequences of this effect for stellar wind diagnostics on the basis of the usually observed UV resonance lines will be investigated in a forthcoming paper.

An important consequence of the non-LTE multi-level calculations and the shift to higher ionization stages is that high ionization species like O VI, S VI, N V can be produced easily in an O-star cool wind model. *Thus the longstanding problem of "superionization" can be solved without any other source of ionization.* This holds at least for objects as hot as ζ Pup ($T_{\rm eff} \approx$ 42,000 K). For very late O-stars like τ Sco at least N V can be easily obtained. At the moment, the calculations still fail margin-

ally to produce the observed amount of O VI in the case of τ Sco. This will be subject to further investigations and additional calculations.

The influence of the improved occupation numbers on the wind dynamics is significant. The shift to higher ionization stages weakens the line force and leads to a mass-loss rate and terminal velocity very close to the observations for ζ Pup. For τ Sco a reasonable mass-loss rate is also found. The velocity field already reaches a value of 2000 km s^{-1} very close to the star. This value is observed with some uncertainty from the shallow blue wings of the UV-profiles. In the outer layers the velocity rises further up to 3850 km s^{-1} but here the ion densities are too small to produce effects on the observable profiles.

From these results we conclude that the concept of radiation driven cool winds is the right way to describe quantitatively the rapidly expanding envelopes of hot stars. Of course, the present work is only a first step. The next one will be to include the effects of multiple scattering in a comparable realistic selfconsistent treatment. At first glance this appears to be a hopeless task, since all multi-level rate equations for the different elements are directly radiatively coupled due to the overlapping line transitions. However, the treatment of the problem within our group (mainly J. Puls with A. Pauldrach and R.P. Kudritzki) is well advanced and first results will be forthcoming soon. With this important effect included, detailed stellar wind model calculations will be undertaken not only for OB-stars but also for Wolf-Rayet stars. For the latter case the results by Pauldrach et al. (1985) indicate that the situation is not completely hopeless.

Another crucial topic is the selfconsistent treatment of the energy balance in the stellar wind. Here one will have to investigate how the radiative equilibrium is affected by the probable energy dissipation in shocks (Lucy and White, 1980; Lucy, 1982). We suggest the use of the detailed and improved wind models for an analysis of the stability of the acceleration mechanism and the wind flow (see Owocki and Rybicki, 1985). The results could then be taken to investigate the shock properties, in particular the EUV- and X-ray radiation field emitted by them (Krolik and Raymond, 1985). This will be of course extremely important for the quantitative reliability of the ionization calculations.

Acknowledgements. I wish to express my thanks to my colleagues Prof. R.P. Kudritzki, J. Puls, Dr. K. Butler for hundreds of intense and extremely helpful discussions and for the careful reading of the manuscript. It is also a pleasure to thank Dr. D. Abbott for providing me with his line list and for very critical, but also very constructive remarks on the first version of this paper. This research was granted by the Deutsche Forschungsgemeinschaft under Ku 474/11-1.

Appendix A

Table A1 shows the elements (column 1) and ionization stages (column 2) considered in the NLTE calculations. In column 3 and 4 the ionization energy of the ground level and the excitation energy of the highest considered level are given for the corresponding ionization stages, respectively.

It should be mentioned that beside the usual packing of fine structure levels for most ionization stages of iron (asterisk) an additional packing of levels was necessary in order to treat the contribution to the line force of these stages correctly. Of course, only those levels have been packed that are not connected by a line transition and whose excitation energy difference is negligible, so that they may be expected to be in LTE with respect to each other because of collisions even at low densities.

Appendix B

1. Photoionization cross-sections

The cross-sections for b-f absorption $\alpha_{ik}(\nu)$ of level i have been used in the usual Seaton approximation given by

$$\alpha_{ik}(\nu) = \alpha_t(\beta(\nu/\nu_t)^{-s} + (1-\beta)(\nu/\nu_t)^{-s-1}) \tag{A1}$$

where t stands for the relevant threshold value.

At the moment we are not in a position to apply for all the levels the correct photoionization cross sections at threshold and the parameters β and s. Thus, an approximation is needed for these values. Hence, for α_t the approximate formula given by Gould (1978) was used

$$\alpha_t = \frac{(2S+1)(2L+1)}{\Sigma(2S+1)(2L+1)}\, 7.907\, 10^{-18}(I_H/I_t)(NE/n) \tag{A2}$$

where I_t and I_H are the ionization potentials of the considered ionization stage of level i and of the hydrogen ground level, respectively. NE is the number of active bound electrons available for photoejection from level i and n is the principal quantum number. As with the ionization energies from the ground levels, both of these values were taken from Moore (1971a, 1970, 1971, 1975, 1980), Bashkin et al. (1975) or Allen (1973); if no information was available there, the values were derived along isoelectronic sequences. The factor including the quantum numbers of the total spin and angular momentum of the lower ionization stage (see also Gould) was, for those cases in which this information was unavailable, approximated by the corresponding hydrogenic value $(2J+1)/(2n^2)$.

We have chosen Eq. (A2) for the threshold value because Gould has shown that this approximation is accurate within a factor of two for the low lying levels of nearly all ionization stages and we have verified that this is nearly correct for excited levels.

Until now, apart from H and He, the parameters β and s have been set generally equal two, since this number is a reasonable approach for many cross-sections. Of course, the main aim for future work will be to include the exact form of all those photoionization cross-sections presently known and needed for our calculations.

2. Collisional excitation and ionization rates

For excitation rates in radiatively permitted transitions the van Regemorter expression was used for q_{ij} as given by Mihalas (1978, Eq. 5-75, 5-76). All other collisional rates were obtained from the formula

$$q_{ij} = \frac{8.631\, 10^{-6}}{g_j T_e^{1/2}}\,\Omega$$

$$q_{ij} = \frac{g_j}{g_i}\, q_{ji} \exp(-h\nu_{ij}/kT_e) \tag{A3}$$

given by Osterbrock (1974). As it is mainly the ratio of the collisional rates given in Eq. (A3) that influence the occupation numbers of excited levels, Ω was set equal 1 in all cases for which

Table A1. Atomic structure of the elements and ionization stages considered in the calculations

Element	Ionization stage	Ioniz. energy of ground level (cm^{-1})	Excitation energy of highest considered level	
H	I	109678.76	106632.6	
He	I	198305.00	186209.3	
	II	438908.67	426821.0	
C	I	90820.42	79323.2	
	II	196664.70	145550.7	
	III	386241.00	358097.8	
	IV	520178.40	471406.8	
N	I	117225.70	99663.9	
	II	238750.50	188937.2	
	III	382703.80	379371.1	
	IV	624866.00	570381.3	
	V	789537.20	713334.8	
O	I	109836.70	99681.3	
	II	283590.90	232602.6	
	III	443193.50	379310.2	
	IV	624382.00	554461.0	
	V	918702.00	612615.6	
	VI	1114010.00	955856.0	
F	I	140553.50	126581.2	
	II	282190.20	240179.2	
	III	505410.00	427624.2	
	IV	703766.40	556216.6	
	V	921450.00	699350.6	
	VI	1267581.00	790418.5	
Ne	I	173931.70	164285.9	
	II	331350.00	279422.9	
	III	514148.00	440064.9	
	IV	783880.00	588021.0	
	V	1019950.00	698516.5	
	VI	1274000.00	771449.2	
Na	I	41449.65	36372.6	
	II	381528.00	364960.0	
	III	578033.00	547910.7	
	IV	797741.00	644140.0	
	V	1118170.00	801950.0	
	VI	1390558.00	924183.9	
Mg	I	61669.14	56968.3	
	II	121267.41	97468.9	
	III	646364.00	546907.8	
	IV	881759.00	797056.0	
	V	1139421.00	764591.0	
	VI	1507520.00	1100146.0	
Al	I	48279.16	45457.2	
	II	151860.40	125866.7	
	III	229453.99	201969.5	
	IV	967783.00	767041.0	
	V	1240600.00	358810.0	
	VI	1536300.00	1174450.0	
Si	I	65743.00	54871.0	
	II	131838.40	108820.9	
	III	270139.30	209504.0	
	IV	364093.10	299676.9	
	V	1345100.00	1105550.0	
	VI	1654800.00	1329900.0	
P	I	88560.00	65787.4	
	II	158550.00	88894.0	
	III	243290.00	191639.5	
	IV	414312.40	298327.0	
	V	524462.90	414684.4	
	VI	1778250.00	1582860.0	
S	I	83559.30	74975.8	
	II	188824.50	119294.7	
	III	282752.00	174036.2	
	IV	381541.40	271010.4	
	V	584700.00	349773.0	
	VI	710194.00	629395.0	
Cl	I	104991.00	91564.3	
	II	192000.00	132191.3	
	III	321936.00	196155.8	
	IV	431226.00	315121.0	
	V	547000.00	423022.0	
	VI	780000.00	578672.0	
A	I	127109.90	115366.9	
	II	222820.00	159706.5	
	III	329965.80	196679.8	
	IV	482400.00	268171.4	
	V	605100.00	301300.0	
	VI	736600.00	342286.0	
K	I	35009.78	31953.2	
	II	256637.00	215018.8	
	III	369000.00	263770.0	
	IV	491300.00	273409.0	
	V	666192.50	292968.0	
	VI	804513.00	223840.0	
Ca	I	49304.80	39340.1	
	II	95748.00	81517.0	
	III	413127.00	290934.3	
	IV	542000.00	337207.0	
	V	680800.00	197849.0	
	VI	879139.90	231318.0	
Ti	I	55138.00	17540.2	
	II	110000.00	25193.0	
	III	227000.00	137971.0	
	IV	348817.80	312973.5	
	V	805500.00	612970.0	
V	I	54361.00	15770.7	
	II	114600.00	19191.5	
	III	240000.00	56922.5	
	IV	391000.00	155565.5	
	V	526000.00	403933.0	
Cr	I	54565.00	25771.4	
	II	133060.00	34813.1	
	III	249700.00	51093.1	
	IV	400000.00	119670.0	
	V	589700.00	239917.5	
	VI	730900.00	383304.0	
Mn	I	59960.00	31124.9	
	II	126147.00	38901.8	
	III	271800.00	72184.8	
	IV	414571.70	112882.8	
	V	613200.00	205126.0	
	VI	782353.80	336126.0	
Fe	I	63700.00	23270.4	
	II	130524.00	39109.3	*
	III	247200.00	89491.4	*
	IV	441993.70	186762.0	*
	V	608945.80	259995.2	*
	VI	806550.40	365494.0	*
Co	I	63438.00	24733.3	
	II	137572.00	42008.6	
	III	270200.00	73861.8	
Ni	I	61579.00	31786.2	
	II	146408.00	58705.9	
	III	283700.00	110371.1	
	IV	442668.20	146194.3	
	V	608945.00	164713.9	
	VI	871074.40	309975.7	
Cu	I	62317.20	43744.4	
	II	163665.60	95565.6	
	III	297100.00	128679.4	
Zn	I	75766.80	68450.1	
	II	144890.60	49370.3	
	III	320300.00	221343.6	

Eq. (A3) was applied. This value is a representative one (see Osterbrock, 1974, p. 46, Table 3.3–3.7).

Finally the collisional ionization cross-sections were expressed in terms of the photoionization cross-sections at threshold derived by Seaton and also given by Mihalas (Eq. 5-79).

Appendix C

To check the influence of collisional rates on the population of the excited levels, we consider the rate equations assuming that all lines are in detailed balance

$$\frac{n_i}{n_1}\left(\sum_{j\neq i}^{n} C_{ij} + R_{ik}\right) = \sum_{j\neq i}^{n} \frac{n_j}{n_1} C_{ji} + \frac{n_k}{n_1} R_{ki} \tag{A4}$$

and insert the ionization equation

$$\sum_j \frac{n_j}{n_1} R_{jk} = \frac{n_k}{n_1} \sum_j R_{kj} \tag{A5}$$

thus we obtain

$$\frac{n_i}{n_1}\left(\sum_{j\neq i}^{n} C_{ij} + R_{ik} - \frac{R_{ik}R_{ki}}{\sum_l R_{kl}}\right) = \sum_{j\neq i}^{n} \frac{n_j}{n_1}\left(C_{ji} + \frac{R_{jk}R_{ki}}{\sum_l R_{kl}}\right) \tag{A6}$$

From Eq. (A6) it is obvious that for any $i \leq i_{\max}$, $n_i/n_1 \approx (n_i/n_1)^*$ if

$$\sum_{j\neq i}^{n} C_{ij} > C_{ij} \gg R_{ik} > R_{ik} - \frac{R_{ik}R_{ki}}{\sum_l R_{kl}}$$

$$C_{ji} \gg R_{jk} > \frac{R_{jk}R_{ki}}{\sum_l R_{kl}} \tag{A7}$$

or

$$C_{ij} \gg R_{ik}\,.$$

In the case $i_{\max} \geq j > i$ we find

$$\frac{C_{ji}}{R_{jk}} \approx \frac{n_e}{W} \frac{1.5\,10^{22}}{\nu_j^2 T_e^{1/2} T_{R_j} \exp(-h\nu_j/kT_{R_j})} \tag{A8}$$

(where Eq. (A3) and (A1) were used assuming $\Omega = 1$ and $\alpha_t = 10^{-18}$, $\beta = s = 2$, respectively), whereas for $j < i \leq i_{\max}$

$$\frac{C_{ji}}{R_{jk}} \approx \frac{C_{ij}}{R_{jk}} \exp(-h\nu_{ij}/kT_e) \tag{A9}$$

we have to distinguish between the cases

i) $\nu_j > \nu_{\mathrm{He\,II}}$ where $T_{Rj} < T_e$ and thus $C_{ji}/R_{jk} > C_{ij}/R_{ik}$ for $\nu_{ij} < \nu_j$

ii) $\nu_j < \nu_{\mathrm{He\,II}}$ where $T_{Rj} \approx T_e$ and thus $C_{ji}/R_{jk} \approx C_{ij}/R_{ik}$

Thus, $i_{\max}$ has to be determined from Eq. (A8).

Assuming the worst case for ζ Pup ($(n_e/W)_{\min} \approx 3\,10^{11}$, $T_R = T_e$) Eq. (A8) gives $C_{ji}/R_{jk} > 1$ for $\lambda_j < 286$ Å. Thus, as this is due to our proceeding from the lower limit, LTE can be obtained for the population of excited levels in cases where $\lambda_j < 300$ Å and the b-b rates are in detailed balance.

References

Abbott, D.C.: 1979, *IAU Symp.* **83**, ed. P.S. Conti, C.W.H. de Loore, p. 237

Abbott, D.C.: 1982, *Astrophys. J.* **259**, 282

Abbott, D.C., Hummer, D.G.: 1985, *Astrophys. J.* **294**, 286

Abbott, D.C., Lucy, L.B.: 1985, *Astrophys. J.* **288**, 679

Aldrovandi, S.M.V., Péquignot, D.: 1973, *Astron. Astrophys.* **25**, 137

Allen, C.W.: 1973, Astrophysical Quantities, 3rd ed. London, Athlone Press

Bashkin, S., Stoner, J.O., 1975, Atomic Energy Levels and Grotrian Diagrams, North-Holland Publishing Company

Bathia, A.K., Underhill, A.B.: 1986, *Astrophys. J. Suppl.* **60**, 323

Bertiau, F.C.: 1958, *Astrophys J.* **128**, 533

Bohannan, B., Abbott, D.C., Hummer, D.G. Voles, S.A.: 1985, in *Luminous Stars and Associations in Galaxies*, Proc. *IAU Symp.* **116**, eds. C. de Loore, A. Willis, P. Laskarides, Reidel, Derdrecht

Cassinelli, J.P., Olson, G.L.: 1979, *Astrophys. J.* **229**, 304

Cassinelli, J.P., Swank, J.H.: 1983, *Astrophys. J.* **271**, 681

Castor, J.: 1970, *Monthly Notices Roy. Astron. Soc.* **149**, 111

Castor, J.: 1974, *Monthyl Notices Roy. Astron. Soc.* **169**, 279

Castor, J., Abbot, D., Klein, R.: 1975, *Astrophys. J.* **195**, 157

Castor, J., Abbott, D., Klein, R.: 1976, *Physique des Mouvements dans les Atmospheres Stellaires*, eds. R. Cayrel, M. Steinberg, Paris, CNRS, p. 363

Castor, J.: 1979, *IAU Symp. No.* **83**, 175

Castor, J., van Blerkom, D.: 1970, *Astrophys. J.* **161**, 485

Deltabuit, E., Cox, O.: 1972, *Astrophys. J.* **177**, 855

Friend, D., Abbott, D.C.: 1987 (in press)

Friend, D., Castor, J.: 1983, *Astrophys. J.* **272**, 259

Gabler, R. et al.: 1986, (in preparation)

Gehren, T., Nissen, P.E., Kudritzki, R.P., Butler, K.: 1985, Proc. ESO Workshop on *Production and Distribution of C, N, O Elements*, Garching, p. 171

Gould, R.J.: 1978, *Astrophys. J.* **219**, 250

Hamann, W.-R.: 1980, *Astron. Astrophys.* **84**, 342

Hamann, W.-R.: 1981, *Astron. Astrophys.* **100**, 169

Hardorp, J., Scholz, M.: 1969, *Astrophys. J. Suppl.* **19**, 193

Hearn, A.: 1975 *Astron. Astrophys.* **40**, 277

Herrero, A.: 1987, *Astron. Astrophys.* (in press)

Holweger, H.: 1979, *Les Elements et leurs Isotopes dans L'Univers*, Universite de Liege, Institut d'Astrophysique

Hummer, D.G., Rybicki, G.B.: 1985, *Astrophys. J.* **293**, 258

Husfeld, D., Kudritzki, R.P., Simon, K., Clegg, R.: 1984, *Astron. Astrophys.* **134**, 139

Jenkins, L.: 1951, *Astron. J.* **55**, 138

Klein, R., Castor, J.: 1978, *Astrophys. J.* **220**, 902

Krolik, J., Raymond, J.: 1985, *Astrophys. J.* **298**, 660

Kudritzki, R.P., Simon, K.P., Hamann, W.R.: 1983, *Astron. Astrophys.* **118**, 245

Kudritzki, R.P., Pauldrach, A. und Puls, J.: 1987, *Astron. Astrophys.* (in press)

Kurucz, R.L.: 1979, *Astrophys. J. Suppl.* **40**, 1

Lamers, H.J.G.L.M., Morton, D.: 1976, *Astrophys. J. Suppl.* **32**, 715

Lamers, H.J.G.L.M., Rogerson, J.B.: 1978, *Astron. Astrophys.* **66**, 417

Lamers, H.J.G.L.M., Waters, L.B., Wesselius, P.R.: 1984, *Astron. Astrophys.* **134**, L17

Long, K.S., White, R.L.: 1980, *Astrophys. J. Letters* **239**, L65

Lucy, L.B., Solomon, P.: 1970, *Astrophys. J.* **159**, 879

Lucy, L.B., White, R.: 1980, *Astrophys. J.* **241**, 300

Lucy, L.B.: 1982, *Astrophys. J.* **255**, 286

Mihalas, D., Hummer, D.: 1973, *Astrophys. J.* **179**, 827
Mihalas, D.: 1978, *Stellar Atmospheres*, W.H. Freeman and Company, San Francisco
Moore, C.E.: 1971a, *Atomic Energy Levels*, NSRDS-NBS 35, Washington, US Dept. of Commerce
Moore, C.E.: 1970, *Selected Tables of Atomic Spectra*, NSRDS-NBS 3, Sect. 3, Washington, US Dept. of Commerce
Moore, C.E.: 1971, *Selected Tables of Atomic Spectra*, NSRDS-NBS 3, Sect. 4, Washington, US Dept. of Commerce
Moore, C.E.: 1975, *Selected Tables of Atomic Spectra*, NSRDS-NBS 3, Sect. 5, Washington, US Dept. of Commerce
Moore, C.E.: 1980, *Selected Tables of Atomic Spectra*, NSRDS-NBS 3, Sect. 9, Washington, US Dept. of Commerce
Nußbaumer, H., Storey, P.J.: 1983, *Astron. Astrophys.* **126**, 75
Nußbaumer, H., Storey, P.J.: 1984, *Astron. Astrophys. Suppl.* **56**, 293
Nußbaumer, H., Storey, P.J.: 1987, *Astron. Astrophys. Suppl.* (in press)
Olson, G.L.: 1978, *Astrophys. J.* **226**, 124
Olson, G.L., Castor, J.: 1981, *Astrophys. J.* **244**, 179
Osterbrock, D.E.: 1974, *Astrophysics of Gaseous Nebulae*, W.H. Freeman and Company, San Francisco
Owocki, S.P., Rybicki, G.B.: 1985, *Astrophys. J.* **299**, 265
Pauldrach, A., Puls, J., Hummer, D.G., Kudritzki, R.P.: 1985, *Astron. Astrophys.* **148**, L1
Pauldrach, A., Puls, J., Kudritzki, R.P.: 1986, *Astron. Astrophys.* **164**, 86
Pauldrach, A.: 1986, Ph.D. Thesis, Munich University
Schönberner, D., Herrero, A., Kudritzki, R.P., Simon, K.P.: 1987, *Astron. Astrophys.* (submitted)
Waldron, W.L.: 1984, *Astrophys. J.* **282**, 256